nature materials

SUPPLEMENTARY INFORMATION

https://doi.org/10.1038/s41563-020-0707-7

In the format provided by the authors and unedited.

Supramolecular–covalent hybrid polymers for light-activated mechanical actuation

Chuang Li[1,7], Aysenur Iscen[2,7], Hiroaki Sai[1], Kohei Sato[1], Nicholas A. Sather[3], Stacey M. Chin[1,4], Zaida Álvarez[1,5], Liam C. Palmer[1,4], George C. Schatz[2,4] ✉ and Samuel I. Stupp[1,3,4,5,6] ✉

[1]Simpson Querrey Institute, Northwestern University, Chicago, IL, USA. [2]Department of Chemical and Biological Engineering, Northwestern University, Evanston, IL, USA. [3]Department of Materials Science and Engineering, Northwestern University, Evanston, IL, USA. [4]Department of Chemistry, Northwestern University, Evanston, IL, USA. [5]Department of Medicine, Northwestern University, Chicago, IL, USA. [6]Department of Biomedical Engineering, Northwestern University, Evanston, IL, USA. [7]These authors contributed equally: Chuang Li, Aysenur Iscen.
✉e-mail: g-schatz@northwestern.edu; s-stupp@northwestern.edu

Supporting Information

Supramolecular–Covalent Hybrid Polymers for Light-Activated Mechanical Actuation

Chuang Li[1†], Aysenur Iscen[2†], Hiroaki Sai[1], Kohei Sato[1], Nicholas A. Sather[3], Stacey M. Chin[1, 4], Zaida Álvarez[1, 6], Liam C. Palmer[1, 4], George C. Schatz[2, 4, *], Samuel I. Stupp[1, 3, 4, 5, 6, *]

Author address

[1] Simpson Querrey Institute, Northwestern University, 303 East Superior Street, Chicago, Illinois 60611, USA.

[2] Department of Chemical and Biological Engineering, Northwestern University, 2145 Sheridan Road, Evanston, IL 60208, USA.

[3] Department of Materials Science and Engineering, Northwestern University, 2220 Campus Drive, Evanston, Illinois 60208, USA.

[4] Department of Chemistry, Northwestern University, 2145 Sheridan Road, Evanston, IL 60208, USA.

[5] Department of Biomedical Engineering, Northwestern University, 2145 Sheridan Road, Evanston, Illinois 60208, USA.

[6] Department of Medicine, Northwestern University, 676 North St. Clair Street, Chicago, Illinois 60611, USA.

† These authors contributed equally to this work

*Correspondence to: g-schatz@northwestern.edu; s-stupp@northwestern.edu

1. **Supplementary_Video_1** A six-arm flat film of the PA (1 wt%) hybrid hydrogel made of nitro-spiropyran with 0.5 mm thickness bends towards a top light source (blue LED, 447 nm, 0.28 mW/cm^2) with a maximum bending of 42.8° first and eventually become flat with further illumination eliminating the contraction gradient. Scale bar is 5 mm.

2. **Supplementary_Video_2** A six-arm flat film of the PA (1 wt%) hybrid hydrogel made of nitro-spiropyran with 0.2 mm thickness bends up to a top light source (blue LED, 447 nm, 0.28 mW/cm^2) with a maximum bending of 74.2° and falls due to orientationally unstable on surfaces. Scale bar is 5 mm.

3. **Supplementary_Video_3** A six-arm flat film of the PA (1 wt%) hybrid hydrogel made of nitro-spiropyran with 1.0 mm thickness bends up to a top light source (blue LED, 447 nm, 0.28 mW/cm^2) with a maximum bending of 25.7° and become flat with further illumination. Scale bar is 5 mm.

4. **Supplementary_Video_4** A six-arm flat film of the PA (1 wt%) hybrid hydrogel with made of nitro-spiropyran 2.0 mm thickness bends up to a top light source (blue LED, 447 nm, 0.28 mW/cm^2) with a maximum bending of 13.9° and become flat with further illumination. Scale bar is 5 mm.

5. **Supplementary_Video_5** A six-arm flat film of soft pure polymer hydrogel made of nitro-spiropyran with comparable crosslink densities (2.8 %) to those in the PA hybrid exhibits low degrees of bending (<5°). Scale bar is 5 mm.

6. **Supplementary_Video_6** A six-arm flat film of stiff pure polymer hydrogel made of nitro-spiropyran with higher crosslink densities (10 %) exhibits a slower response to light. Scale bar is 5 mm.

7. **Supplementary_Video_7** A six-arm flat film of soft pure polymer hydrogel made of nitro-spiropyran blended with glass fiber (5 wt%) exhibits a slower response to light. Scale bar is 5 mm.

8. **Supplementary_Video_8** A six-arm flat film of the PA (0.5 wt%) hybrid hydrogel made of nitro-spiropyran with 0.5 mm thickness bends towards a top light source (blue LED, 447 nm, 0.28 mW/cm^2) with a maximum bending of 39.4° first and eventually become flat with further illumination eliminating the contraction gradient. Scale bar is 5 mm.

9. **Supplementary_Video_9** A six-arm flat film of the PA (1.5 wt%) hybrid hydrogel made of nitro-spiropyran with 0.5 mm thickness bends towards a top light source (blue LED, 447 nm, 0.28 mW/cm^2) with a maximum bending of 36.0° first and eventually become flat with further illumination eliminating the contraction gradient. Scale bar is 5 mm.

10. **Supplementary_Video_10** A six-arm flat film (0.5 mm thick) made of nitro-spiropyran with the aligned PA (1 wt%) fibers by 3D printing bends towards a top light source (blue LED, 447 nm, 0.28 mW/cm^2) with a maximum bending of 44.2° first and eventually become flat in 34 min with further illumination eliminating the contraction gradient. Scale bar is 5 mm.

11. **Supplementary_Video_11** A six-arm flat film (0.5 mm thick) made of nitro-spiropyran with the non-aligned PA (1 wt%) fibers by casting bends towards a top light source (blue LED, 447 nm, 0.28 mW/cm^2) with a maximum bending of 44.0° first and eventually become flat in 48 min with further illumination eliminating the contraction gradient. Scale bar is 5 mm.

12. **Supplementary_Video_12** A four-arm flat film of the PA (1 wt%) hybrid hydrogel made of nitro-spiropyran walks unidirectionally from left to right on a poly(dimethyl siloxane) (PDMS) surface

(0.7 mm spacing, 0.5 mm height) during a bending/flattening cycle with bottom light (8.89 mW/cm^2) in 30 min (its centroid moving 2.2 mm). Scale bar is 5 mm.

13. **Supplementary_Video_13** A four-arm flat film of soft pure polymer hydrogel made of nitro spiropyran walks slower from left to right on a poly(dimethyl siloxane) (PDMS) surface (0.7 mm spacing, 0.5 mm height) during a bending/flattening cycle with bottom light (8.89 mW/cm^2) in 30 min (its centroid moving 0.5 mm). Scale bar is 5 mm.

14. **Supplementary_Video_14** A four-arm flat film of the PA (1 wt%) hybrid hydrogel made of a spiropyran without nitro substituent walks unidirectionally from left to right on a poly(dimethyl siloxane) (PDMS) surface (0.7 mm spacing, 0.5 mm height) during a bending/flattening cycle with bottom light (8.89 mW/cm^2) in 20 min (its centroid moving 2.6 mm). Scale bar is 5 mm.

15. **Supplementary_Video_15** A four-arm flat film of soft pure polymer hydrogel made of a spiropyran without nitro substituent walks slower from left to right on a poly(dimethyl siloxane) (PDMS) surface (0.7 mm spacing, 0.5 mm height) during a bending/flattening cycle with bottom light (8.89 mW/cm^2) in 20 min (its centroid moving 1.1 mm). Scale bar is 5 mm.

16. **Supplementary_Video_16** Five steps of unidirectional motion on a ratcheted poly(dimethyl siloxane) (PDMS) surface by the PA (1 wt%) hybrid actuator made of nitro-spiropyran after alternating periods of light on (30 min) and light off (10 h). Scale bar is 5 mm.

17. **Supplementary_Video_17** Five steps of unidirectional motion on a ratcheted poly(dimethyl siloxane) (PDMS) surface by the PA (1 wt%) hybrid actuator made of a spiropyran without nitro substituent after alternating periods of light on (20 min) and light off (1.5 h). Scale bar is 5 mm.

18. **Supplementary_Video_18** A PA (1 wt%) hybrid crawler made of nitro spiropyran with supramolecular PA fibers aligned parallel to the crawling direction using 3D printing walks from left to right on a poly(dimethyl siloxane) (PDMS) surface (0.7 mm spacing, 0.5 mm height) during a bending/flattening cycle with bottom light (8.89 mW/cm^2) in 30 min (its centroid moving 4.7 mm). Scale bar is 5 mm.

19. **Supplementary_Video_19** A PA (1 wt%) hybrid crawler made of nitro spiropyran with supramolecular PA fibers aligned perpendicular to the crawling direction using 3D printing walks from left to right on a poly(dimethyl siloxane) (PDMS) surface (0.7 mm spacing, 0.5 mm height) during a bending/flattening cycle with bottom light (8.89 mW/cm^2) in 30 min (its centroid moving 1.8 mm). Scale bar is 5 mm.

20. **Supplementary_Video_20** A PA (1 wt%) hybrid crawler made of nitro spiropyran with non-aligned supramolecular PA fibers using casting walks from left to right on a poly(dimethyl siloxane) (PDMS) surface (0.7 mm spacing, 0.5 mm height) during a bending/flattening cycle with bottom light (8.89 mW/cm^2) in 30 min (its centroid moving 3.5 mm). Scale bar is 5 mm.

21. **Supplementary_Video_21** Rotational motion of a four-arm PA (1 wt%) hybrid hydrogel actuator made of nitro-spiropyran on a ratcheted poly(dimethyl siloxane) (PDMS) surface. Three cycles of the actuator were shown after alternating periods of light on (30 min) and light off (10 h). Scale bar is 5 mm.

Outline

S1. **Synthesis of peptide amphiphile (PA) and methacrylate-spiropyran**

Solid-phase synthesis of PA

Fmoc deprotections were performed with 30% 4-methylpiperidine in DMF solution for 10 min. Mtt deprotection was performed with trifluoroacetic acid (TFA)/triisopropylsilane (TIS)/dichloromethane in a ratio of 5:1:94 for 5 min. Amino acid coupling reactions were carried out using a coupling mixture of amino acid/HBTU/DIEA (4 : 3.95 : 6 relative to the resin) in DMF. Cleavage of the peptides from the resin was carried out with a mixture of TFA/TIS/H_2O in a ratio of 95:2.5:2.5 for 3 hours. After remove of excess TFA by rotary evaporation, the remaining peptide solution was triturated with cold diethyl ether to obtain a slightly yellow precipitate solid, followed drying under vacuum overnight. The peptides were purified by preparative reverse phase HPLC using a Phenomenex Gemini column (C_{18}, 10 μm, 100 Å, 30×150 mm) at 25 ºC on a Varian Prostar Model 210 preparative HPLC system. Water/acetonitrile gradient containing 0.1 vol % NH_4OH was used as an eluent at a flow rate of 25 mL/min. The purified fractions were collected and concentrated by rotary evaporation to remove acetonitrile, then lyophilized and stored at -20 ºC. Products were characterized by electrospray ionization mass spectrometry (ESI-MS) using an Agilent 6510 quadrupole time-of-flight (Q-TOF) instrument, with 0.1% NH_4OH in a water/acetonitrile mix (70:30) as eluent.

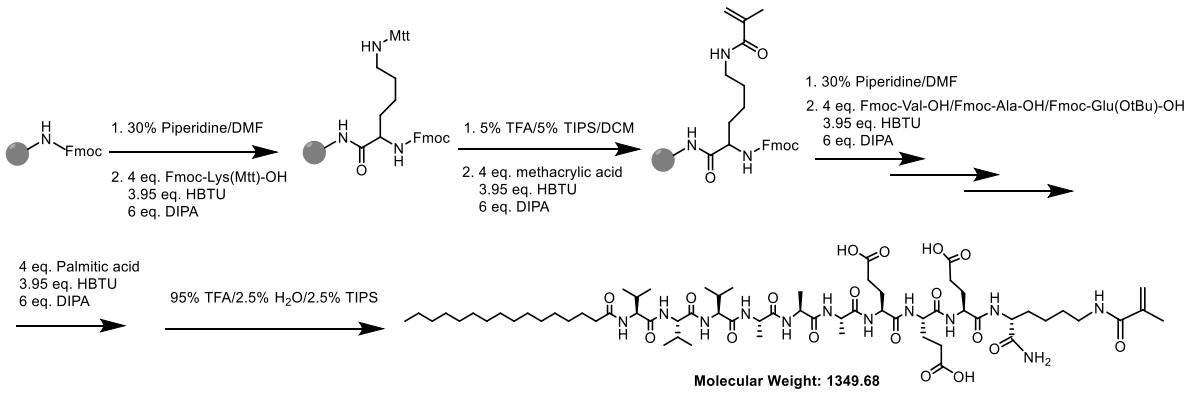

In total, four peptide sequences were synthesized and characterized:

PA 1: C_{16}VVVAAAEEEK-Methacrylamide, Calc. 1349.68, found $[M+H]^+$ 1349.97.
PA 2: C_{16}VVVAAAEEE-NH_2, Calc. 1153.43, found $[M+Na]^+$ 1175.71.
PA 3: C_{16}VVVAAAEEEK-Isobutyramide, Calc. 1351.69, found $[M+Na]^+$ 1374.03.
PA 4: C_{16}VVVAAAEEEK-Tetramethylrhodamine, Calc. 1695.06, found $[M+H]^+$ 1696.27.

Synthesis and characterization of methacrylate-spiropyran

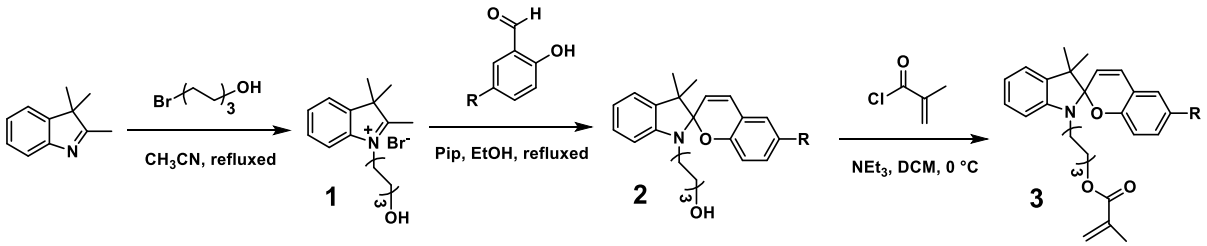

Synthesis of 1-(6-hydroxyhexyl)-2, 3, 3-trimethyl-3H-indole-1-ium bromide (1).
2,3,3-trimethyl-3*H*-indolenine (2.0 g, 12.4 mmol) and 6-bromo-1-hexanol (2.9 g, 16.2 mmol) were dissolved in 20 mL acetonitrile, followed by stirring for 24 h at 85 °C under reflux. Afterwards the mixture was slowly cooled to room temperature and acetonitrile was removed under reduced pressure to get dark red oil. After complete drying under high vacuum overnight, the product was dissolved in 50 mL dichloromethane and extracted three times with deionized (DI) water (3×50 mL). The aqueous phase was carefully concentrated by rotary evaporation at 60 °C to remove water, followed by complete drying under high vacuum to obtain a red dark salt (3.3 g, 78%).
^{1}H-NMR (400 MHz, *d_6*-DMSO) δ (ppm): 7.99 (m, 1H), 7.85 (m, 1H), 7.63 (m, 2H), 4.46 (t, 2H), 3.39 (t, 2H), 2.85 (s, 3H), 1.84 (m, 2H), 1.55 (s, 6H), 1.33-1.48 (m, 6H).
MS-ESI (m/z): $[M-Br]^+$ calc. for $C_{17}H_{26}NO$ 260.40; found 260.09.

Synthesis of 6-(3', 3'-dimethyl-6-nitrospiro [chromene-2, 2'-indoline]-1'-yl) hexan-1-ol (2a).
2,3,3-trimethylindoleninalcohol (**1**, 1.0 g, 3.5 mmol) and 2-hydroxy-5-nitrobenzaldehyde (0.89 g, 5.35 mmol) were added to 30 mL of ethanol, followed by addition of piperidine (0.38 mL, 3.8 mmol). The reaction mixture was stirred at 80 °C under reflux for 24 h. After cooling down to room temperature, the solvent is removed under reduced pressure and the raw product is purified via silica gel column chromatography by using hexanes/ethyl acetate (5:1) as eluent. After complete drying under vacuum overnight, 1.07 g (2.6 mmol) of a pink solid (**2a**) with a yield of 75 % was obtained.
^{1}H-NMR (400 MHz, $CDCl_3$) δ (ppm): 8.04-7.98 (m, 2H,), 7.18 (t, 1H), 7.08 (d, 1H), 6.89 (t, 2H), 6.74 (d, 1H), 6.57 (d, 1H), 5.86 (s, 1H), 3.62 (t, 2H), 3.22-3.09 (m, 2H), 1.63-1.49 (m, 4 H), 1.40-1.31 (m, 4H), 1.28 (s, 3H), 1.18 (s, 3H).
MS-ESI (m/z): [M] calc. for $C_{24}H_{28}N_2O_4$ 408.50; $[M+H]^+$ found 409.17.

Synthesis of 6-(3', 3'-dimethyl-spiro [chromene-2, 2'-indoline]-1'-yl) hexan-1-ol (2b).
2b was synthesized following the same protocol as 2a.
^{1}H-NMR (400 MHz, $CDCl_3$) δ (ppm): 7.32-7.15 (m, 2H,), 7.12-7.03 (m, 3H), 6.84 (t, 2H), 6.70 (d, 1H), 6.55 (d, 1H), 5.69 (s, 1H), 3.62 (t, 2H), 3.29-3.06 (m, 2H), 1.72-1.41 (m, 8H), 1.31 (s, 3H), 1.18 (s, 3H).
MS-ESI (m/z): [M] calc. for $C_{24}H_{29}NO_2$ 363.50; $[M+H]^+$ found 364.22.

Synthesis of 6-(3', 3'-dimethyl-6-nitrospiro[chromene-2,2'-indolin]-1'-yl) hexyl methacrylate (3a).
6-(3', 3'-dimethyl-6-nitrospiro [chromene-2, 2'-indoline]-1'-yl) hexan-1-ol (**2a**, 1.2 g, 2.94 mmol) was dissolved in 40 mL of dichloromethane, followed by addition of NEt_3 (1.2 mL, 8.5 mmol) in one portion. The reaction mixture was cooled to 0 °C followed by drop-wise addition of methacryloyl chloride (0.83 mL, 8.5 mmol). After keeping the reaction at 0 °C for an additional hour, the mixture was stirred at room temperature for 24 h. The product was purified by column chromatography (3:2 dichloromethane/hexanes) to obtain **3** (0.64 g, 1.35 mmol, 46%) as dark-yellow solid.
^{1}H-NMR (400 MHz, $CDCl_3$) δ (ppm): 8.04-7.97 (m, 2H), 7.18 (dd, 1H), 7.08 (d, 1H), 6.94-6.83 (m, 2H), 6.74 (d, 1H), 6.56 (d, 1H) 6.07 (s, 1H), 5.85 (d, 1H), 5.54 (s, 1H), 4.11 (m, 2H), 3.21-3.08 (m, 2H), 1.93 (s, 3H), 1.71-1.59 (m, 4 H), 1.44-1.33 (m, 4H), 1.28 (s, 3H), 1.18 (s, 3H).
MS-ESI (m/z): [M] calc. for $C_{28}H_{32}N_2O_5$ 476.57; $[M+Na]^+$ found 499.17.

Synthesis of 6-(3', 3'-dimethyl-spiro[chromene-2,2'-indolin]-1'-yl) hexyl methacrylate (3b).
3b was synthesized following the same protocol as 3a.
^{1}H-NMR (400 MHz, $CDCl_3$) δ (ppm): 7.95 (dd, 1H), 7.70-7.65 (m, 1H), 7.18 (dd, 1H), 7.05 (d, 1H), 6.86-6.80 (m, 2H), 6.70 (d, 1H), 6.55 (d, 1H), 6.45 (t, 1H) 6.12-6.08 (m, 1H), 5.87 (t, 1H), 5.56 (t, 1H), 4.13 (m, 2H), 3.29-3.07 (m, 2H), 1.96 (s, 3H), 1.71-1.59 (m, 4 H), 1.44-1.33 (m, 4H), 1.31 (s, 3H), 1.18 (s, 3H).
MS-ESI (m/z): [M] calc. for $C_{28}H_{33}NO_3$ 431.58; $[M+Na]^+$ found 454.38.

S2. **Co-assembly and characterization of PAs**

(Cryogenic) Transmission Electron Microscopy ((cryo-)TEM)

TEM was performed on H8100 Transmission Electron Microscope, operating at 200 kV. Samples were stained by 1 wt % uranyl acetate aqueous solution on the surface of carbon-coated copper grids. Plunge-freezing for cryo-TEM samples were performed using a FEI model Vitrobot Mark III. 6.5 µL of sample solution was deposited on a plasma-cleaned copper TEM grid with holey carbon support film (Electron Microscopy Science) and held in place with tweezers mounted on the Vitrobot. The specimen was blotted in an environment with 100% humidity at 22 °C (blot offset: 0.5 mm, blot total: 1, wait time: 0 sec, blot time: 5 secs, drain time: 0 sec), and plunged into a liquid ethane reservoir cooled by liquid nitrogen. The vitrified samples were stored in liquid nitrogen and then transferred to a Gatan cryo-TEM holder. Cryo-TEM images were obtained using a Hitachi model HT-7700 electron microscope operating with an accelerating voltage of 120 kV, equipped with an Orius SC 1000A camera.

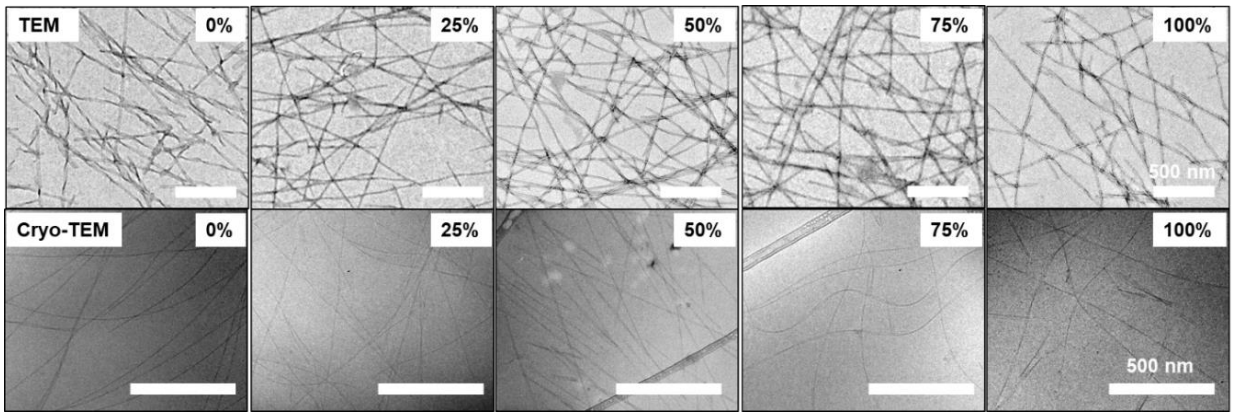

Supplementary Figure 1 Representative TEM and cryo-TEM images of cylindrical fibers formed by PA co-assembly with variable methacrylamide-PA (PA1) ratios from 0% to 100%. Top: conventional TEM images; bottom: Cryo-TEM images. The scale bar is 500 nm.

Circular Dichroism (CD) Spectroscopy

CD spectra were obtained at 25 °C on a Jasco J-715 CD in the Keck Biophysics Facility at Northwestern University using 2 mm quartz cuvettes. Each sample was prepared as a solution with a concentration of 50 µM in MilliQ-water.

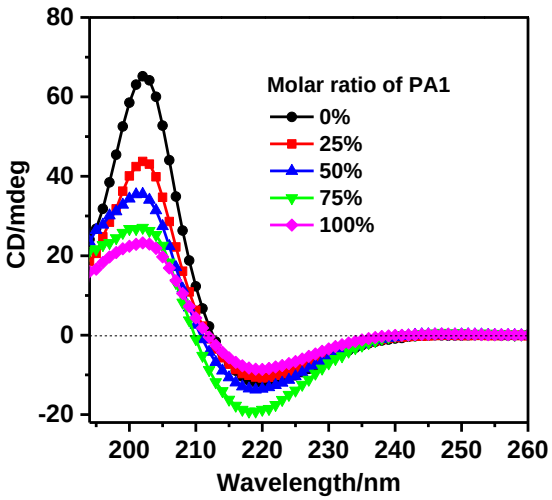

Supplementary Figure 2 Circular dichroism spectra of PA co-assembling solutions (PA1+PA2, 50 μM in total) with various molar ratios of methacrylamide-PA (PA1) relative to PA2 in water at 25 °C.

Fourier-transform infrared (FTIR) spectroscopy

Transmission FT-IR spectra were acquired on a Bruker Tensor 37 FTIR Spectrometer. PA hybrid hydrogel thin films were prepared following the same procedure and lyophilized. These dried films were directly observed in transmission mode. PA (1 wt%) hybrid materials made of different molar ratio of PA1/PA2 (0/1, 1/1, 1/0) were measured. NIPAM monomer or PA powders were grinding with potassium bromide (KBr) powder followed by pressing into a disk before observed in transmission mode. The disappearance of the C=C stretching at 1710 cm^{-1} and =C-H bending at 917 cm^{-1} and 1004 cm^{-1} showed that there were no free methacrylate groups left in the PA hybrid materials.

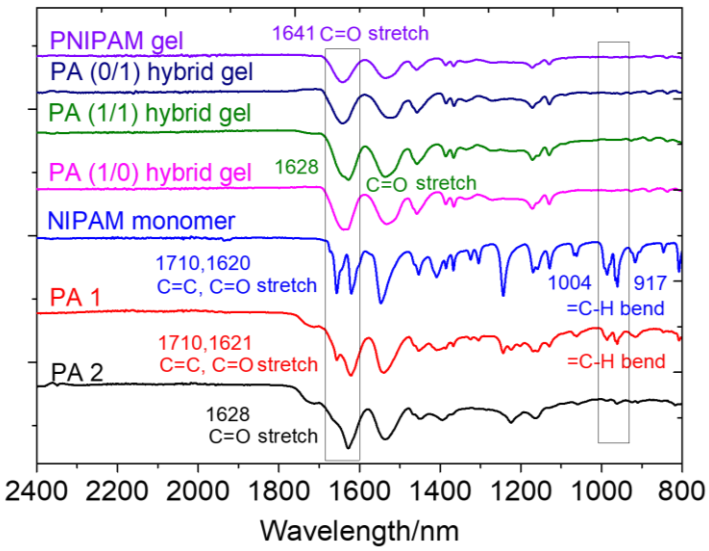

Supplementary Figure 3 Transmission FT-IR spectra of lyophilized hydrogel samples including PNIPAM gel and PA (1 wt%) hybrid gels made of different molar ratios of PA1/PA2 (0/1, 1/1, 1/0). Monomers including NIPAM, PA1 and PA2 were ground into a pellet with potassium bromide (KBr) before measurement. C=C stretching at 1710 cm^{-1} and =C-H bending at 917 cm^{-1} and 1004 cm^{-1} are indicated by rectangles.

^{1}H NMR spectroscopy

To measure the molar ratio between NIPAM and spiropyran monomers, a solution with exact monomer/crosslinker composition as the hydrogel procedure but without crosslinking agent or PA nanofibers was polymerized followed by dissolved in $CDCl_3$ before taking ^{1}H nuclear magnetic resonance (NMR) spectrum on an Agilent DD 600 MHz with a HCN cryoprobe.

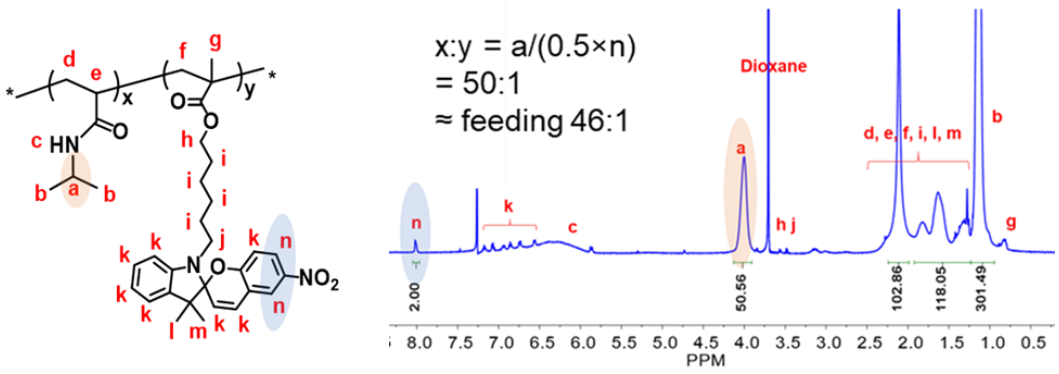

Supplementary Figure 4 ^{1}H Nuclear magnetic resonance (NMR) spectrum of polymerization solution with exact monomer/crosslinker composition as the hydrogel procedure but without crosslinking agent or PA nanofibers, giving a NIPAM/SP molar ratio of 50:1.

Gel permeation chromatography (GPC)

A polymerizable stock solution was prepared without any MBAAm crosslinking agent or PA nanofibers following the hydrogel preparation procedure above. Polymerization of this solution was initiated under the same conditions as hydrogel preparation protocol, resulting in a viscous solution rather than a gel. We assume that the kinetic chain lengths are similar between the solution and hydrogel polymerization conditions. Aliquots of this solution were taken and diluted with *N*, *N*-dimethylformamide (DMF) for size exclusion chromatography in DMF using a Varian PolyPore 300 × 7.5 mm column (flow rate 1 mL min^{-1}), giving a molecular weights (M_w) of 74,000 and PDI of 1.6.

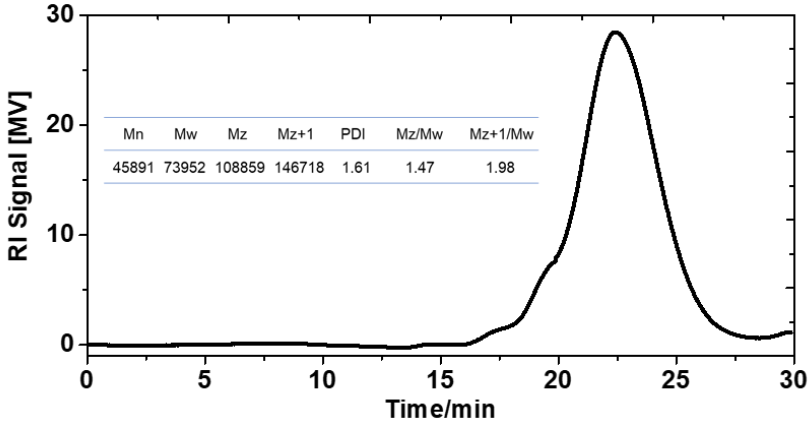

Supplementary Figure 5 Gel permeation chromatography (GPC) trace of polymerization solution with exact monomer/crosslinker composition as the hydrogel procedure but without crosslinker or PA nanofibers, giving a molecular weight (M_w) of 73,952 and PDI of 1.61. The eluent is dimethylformamide (DMF). The molecular weight standards in the GPC were poly(methyl methacrylate) (PMMA) ReadyCal Set.

S3. Preparation and characterization of PA hybrid hydrogels

Hydrogel preparation

To prepare the hybrid hydrogel as an example, *N*-isopropylacrylamide (NIPAM, 21.0 mg, 185.6 μmol), *N*,*N*-methylenebisacrylamide (MBAAm, 0.8 mg, 5.2 μmol), methacrylate-spiropyran (1.9 mg, 4.0 μmol), methacrylate-PA/filler PA (molar ratio of 1/1, 2.1 mg, 1.7 μmol) were dissolved in dioxane/water solvent (4/1, v/v, 210 μL). After annealing in water bath (heating at 80 ºC for 30 min, then cooled down to room temperature overnight), a physical gel was obtained, followed by agitation with a Vortex mixer to break the physical gel. Then 10 wt% of ammonium persulfate initiators (APS, 21.7 μL) and tetramethylethylenediamine (TEMED, 1.4 μL) were added into the solution to start the polymerization at room temperature for 2 h. To remove organic solvent and any unreacted molecules, the resultant gel was soaking in a large volume of MeOH for 24 h during which the soaking MeOH was changed to fresh ones every 4 h. After that, the gel was soaked in acidic water (5 mM HCl) for another 24 h to get the final hydrogel. Specific hydrogel samples were prepared following the same procedure by varying hydrogel shapes, PA co-assembly ratio or PA contents.

i. To prepare hydrogel films with different thickness, the polymerization solution was added to glass molds with different thickness of spacers. Hydrogel films were then cut into desired shapes and size manually according to desired patterns.
ii. Hydrogel films with different molar ratio of PA 1 were prepared, keeping the total weight percent of PA at 1 wt%.
iii. Hydrogel films with different PA contents (0 wt%, 0.5 wt%, 1.0 wt%, 1.5 wt%, 2.0 wt%) were prepared following the same protocol, keeping the molar ratio of PA 1 at 50%.
iv. Hydrogel films with desired shapes like six-petal flower or four-arm walker were obtained by cutting the gel film into desired shaped according to a printed pattern by manually blading.
v. Hydrogel films blended with glass fibers were prepared by adding glass fiber (10 μm in diameter, hundred μm in length) into the monomer solution followed by shaking homogeneously and then polymerized following the same protocol.

Confocal Microscopy

Confocal imaging was done using a Nikon A1R confocal laser-scanning microscope. The hydrogel sample was placed on the glass coverslip and observed with a fluorescein isothiocyanate (FITC) filter and red filter. Z-stacks were done to give a 3D imaging of the hydrogel.

Imaging/analysis of bundles: Fluorescent preparations were viewed, and micrographs were captured with a Nikon A1R confocal laser-scanning microscope with GaAsP detectors and Nikon Structured illumination microscopy (SIM). Images were assembled in Adobe Photoshop (v. 7.0), with adjustments for contrast, brightness, and color balance to obtain optimum visual reproduction of data. Confocal images were also reconstructed by the Imaris program (version 8.1, Bitplane scientific software) for 3D interactive data viewing with normal or shadow projections of PA fiber bundles. The analyses of fluorescence were performed using ImageJ software (National Institutes of Health, USA). For quantification of fluorescently PA bundles samples, a minimum of 30 randomly selected images were included.

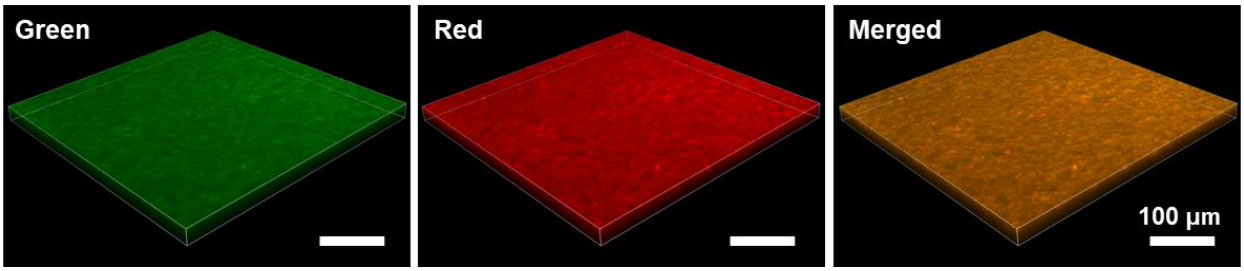

Supplementary Figure 6 Confocal microscopy images of PA-polymer hybrid hydrogel networks with polymer chains labeled by fluorescein (green), PA fibers labeled by 5-carboxytetramethylrhodamine (5-TAMRA, red). Left, green channel; middle, red channel; right, merged.

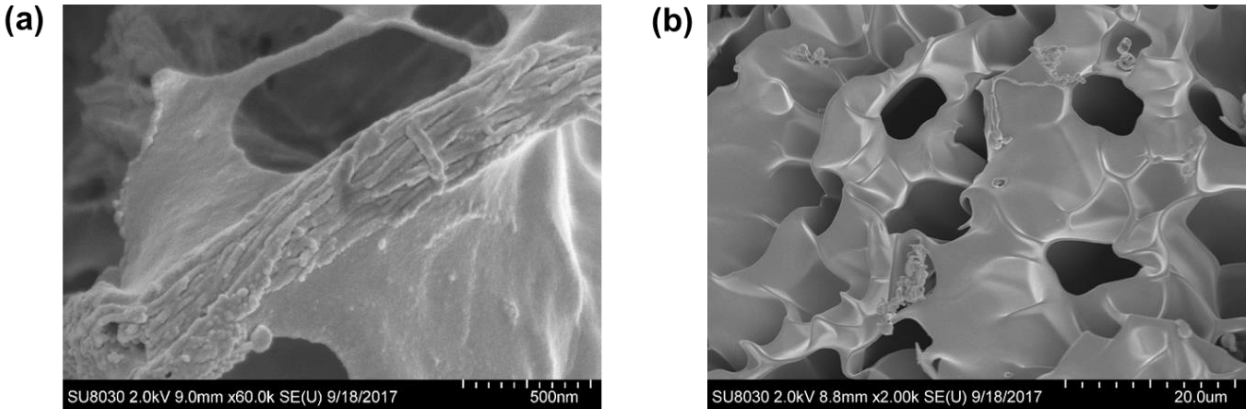

Supplementary Figure 7 SEM images of lyophilized hydrogel samples. (a) Hybrid hydrogel samples and (b) pure polymer hydrogel sample.

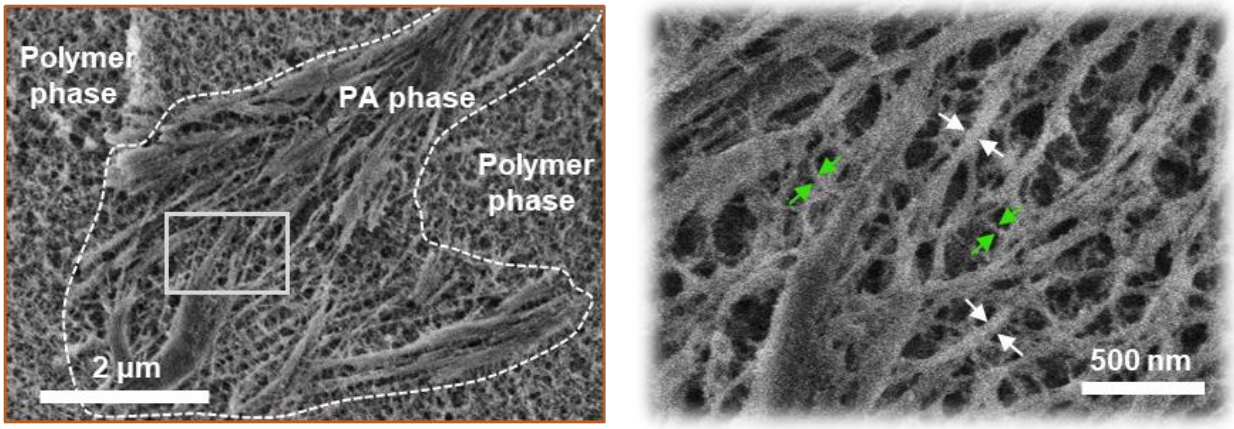

Supplementary Figure 8 Cryo-SEM images of high-pressure frozen hybrid hydrogel sample. Zoom in image was shown in the right. Large fiber bundles and small individual fiber were highlighted by white arrows and green arrows, respectively.

Calculation of the molar ratio of two isomers

To calculate the molar ratio of ring-opened (merocyanine) and ring-closed (spiropyran) forms in the starting material, the spiropyran molecule (compound **3**) was dissolved in a mixture of 1,4-dioxane-d_8/deuterium oxide (4/1, v/v) containing 5 mM DCl and left in the dark overnight before measuring the ^{1}H NMR spectra on an Agilent DD 600 MHz w/HCN cryoprobe. We used ^{1}H-^{1}H NOESY (Nuclear Overhauser Effect Spectroscopy) to confirm that the conformation of the ring-opening merocyanine form in our system is 100% of the *E* isomer of MCH$^+$ based on the observation of e'-i' coupling (no j'-i' coupling was observed). The same sample was irradiated for 30 min with the same light intensity of blue LED (447 nm, 8.89 mW/cm^2) as used for crawling study and measured ^{1}H NMR again on the same instrument. Chemical shifts are relative to the solvent signal. The molar ratio of SP/MCH$^+$ is calculated based on either the decrease in the integration of old peaks (f, g) or the integration of new peaks (f', g') in the dark compared to the total integration of peaks (f, g) in light, giving a molar percentage of MCH$^+$ at the starting material as 33.5%.

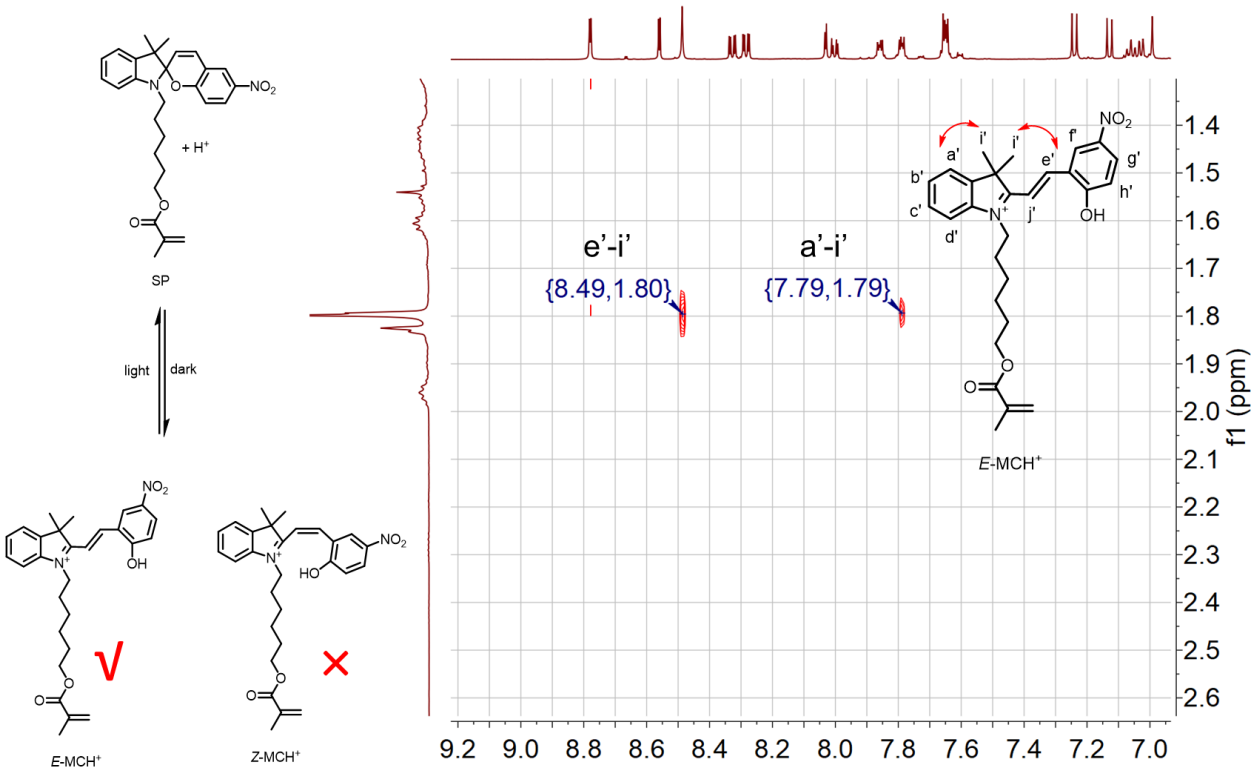

Supplementary Figure 9 Left, chemical structures of ring-closed spiropyran form (SP) and ring-opened protonated merocyanine form (MCH$^+$, both *E* and *Z* isomers); Right, ^{1}H–^{1}H NOESY (Nuclear Overhauser Effect Spectroscopy) of spiropyran molecule with the nitro substituent (10 mg in 1,4-dioxane-d_8/deuterium oxide (4:1, v/v) containing 5 mM DCl) in the dark.

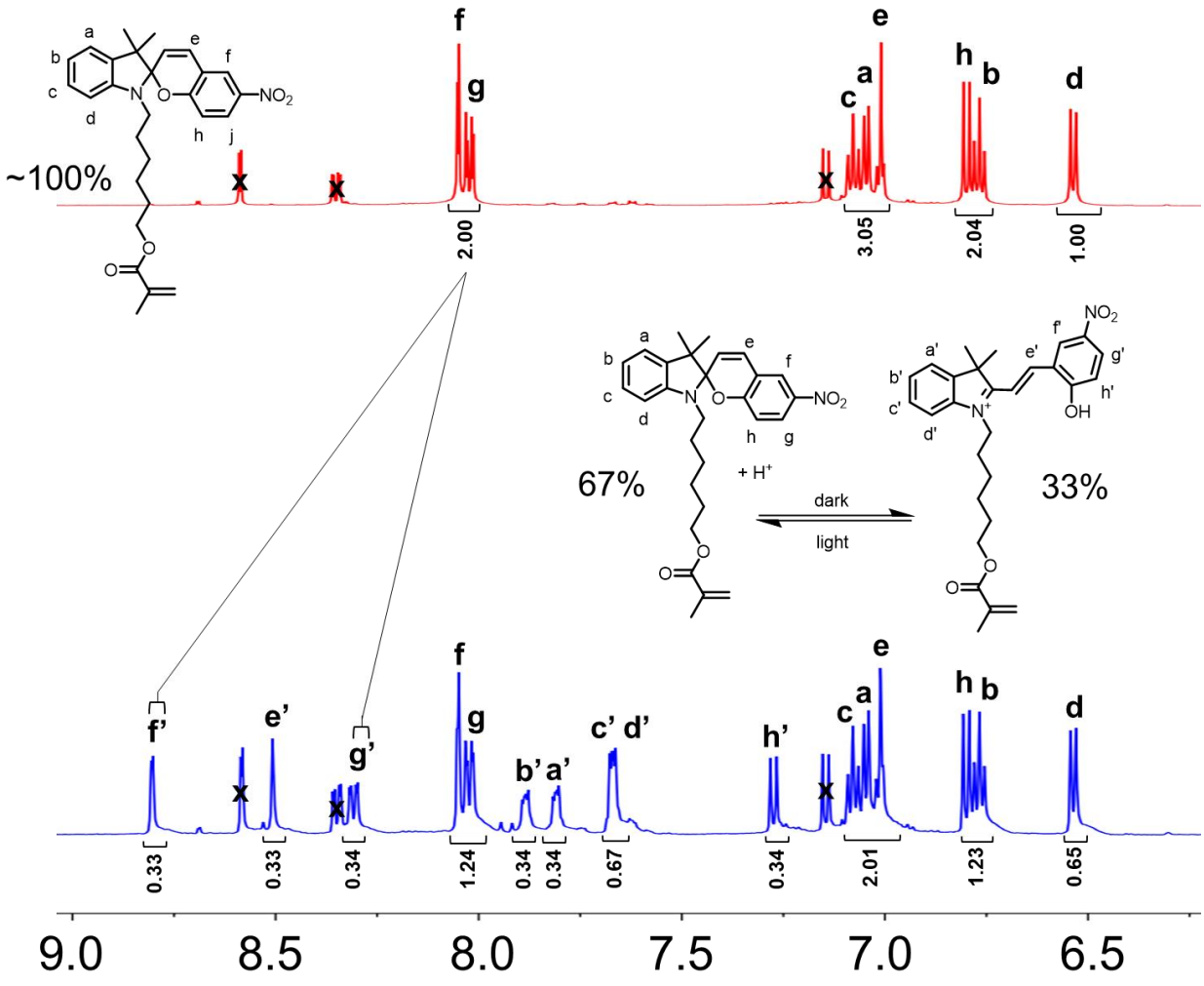

Supplementary Figure 10 ^{1}H-NMR spectra of spiropyran molecule with the nitro substituent (10 mg in 1,4-dioxane-d_8/deuterium oxide (4/1, v/v) containing 5 mM DCl) was measured in the dark (top, blue) and after light irradiation (bottom, red).

UV-Vis spectroscopy

Spiropyran (0.1 mM) was dissolved in a solvent mixture of methanol/water (4/1, v/v) containing 5 mM HCl and incubated in the dark overnight before the measurement. Absorbance spectroscopy of this solution was collected using a 1 mm path length, demountable quartz cuvette on a Shimadzu UV-1800 UV Spectrophotometer. The sample was re-measured with the same intensity of blue light as used in our other experiments (447 nm, 8.89 mW/cm^2). This process was repeated every minute until the absorbance did not change (25 min in total). Plotting the absorbance of the nitro-spiropyran at 414 nm (MCH^+) and the spiropyran without the nitro substituent at 430 nm over irradiation time resulted the photoactuation kinetics, which as fitted by using single exponential (exp1p2) in OriginPro software, giving a photoisomerization rate constant of 0.17228 min^{-1} for the nitro-spiropyran and 0.10427 min^{-1} for spiropyran without the nitro substituent.

To determine the molar absorption coefficient of the spiropyran molecules, we measured the UV-Vis spectra for solution samples with variable concentrations following the protocol described above. After irradiation with light, the molar absorption coefficient of the ring-closed SP form was obtained by linear fitting in OriginPro software, giving a value of 1.5×10^4 L·mol^{-1}·cm^{-1} for the nitro-spiropyran and 1.0×10^4 L·mol^{-1}·cm^{-1} for the spiropyran molecule without the nitro substituent.

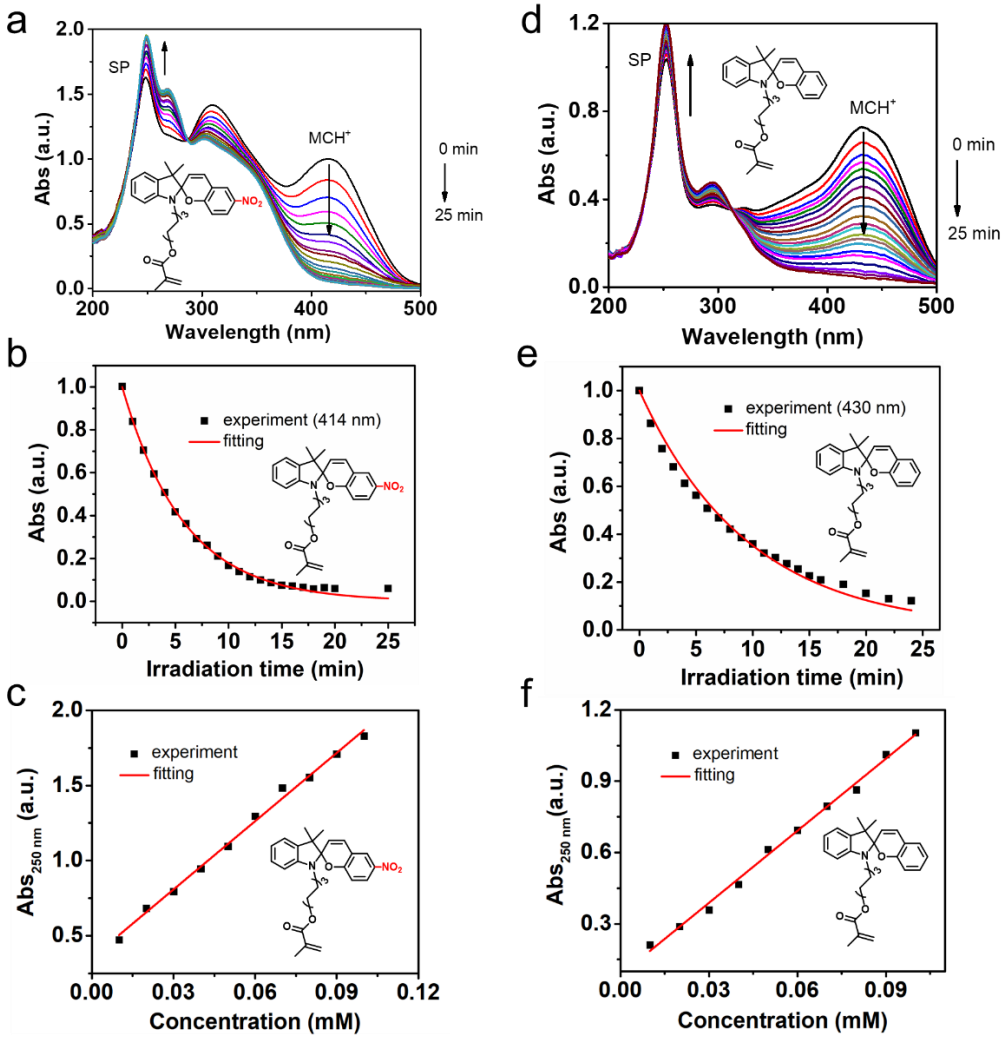

Supplementary Figure 11 **(a)** Absorbance change of the nitro-spiropyran molecule (3a, 0.1 mM) in methanol/water (4/1, v/v) containing 5 mM HCl by irradiating blue light (447 nm, 8.89 mW/cm^2) measured over 25 min. **(b)** Plot of the absorbance at 414 nm (MCH$^+$) of nitro-spiropyran vs irradiation time (back squares) and fitting curve (red line) by using single exponential (exp1p2) in OriginPro software. **(c)** Plot of the absorbance at 450 nm (SP) of nitro-spiropyran vs concentration (black squares) and linear fitting curve (red line) in OriginPro software. **(d)** Absorbance change of the spiropyran molecule without the nitro substituent (3b, 0.1 mM) in methanol/water (4/1, v/v) containing 5 mM HCl by irradiating blue light (447 nm, 8.89 mW/cm^2) measured over 25 min. **(e)** Plot of the absorbance at 430 nm (MCH$^+$) of spiropyran molecule without the nitro substituent vs irradiation time (back squares) and fitting curve (red line) by using single exponential (exp1p2) in OriginPro software. **(f)** Plot of the absorbance at 450 nm (SP) of spiropyran without nitro substituent vs concentration (black squares) and linear fitting curve (red line) in OriginPro software.

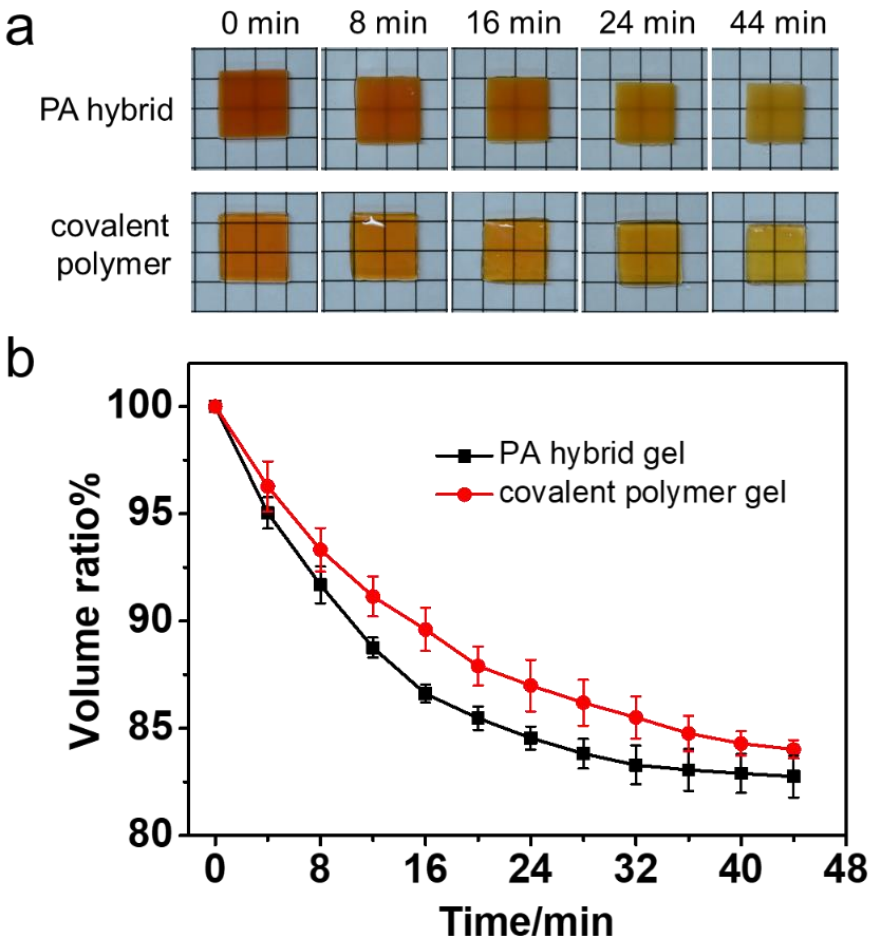

Supplementary Figure 12 Contraction kinetics of the PA hybrid hydrogel and the covalent polymer hydrogel made of nitro-spiropyran. **(a)** Photographs of PA hybrid hydrogel (top) and covalent polymer hydrogel (bottom) by irradiating light (8.89 mW/cm^2) for different times. **(b)** Plot of the contraction kinetics obtained by measuring the area change of photographs in (a) by ImageJ. Error bars represent standard deviations of data collected from three separate samples.

To calculate the optical density, we prepared hydrogel thin films with a thickness of 0.05 mm and these samples were stored in acidic solution (5 mM of HCl) in the dark overnight to reach the equilibrium state of the $MCH^+ \leftrightarrow SP$. Absorbances at 447 nm of these samples were collected using a Shimadzu UV-1800 UV Spectrophotometer to obtain the optical density in the dark. After irradiation with blue light for 5 min to trigger the isomerization from merocyanine to spiropyran form, the absorbances at 447 nm of these samples were collected again, giving the optical density in the light. The detailed values of the measured optical densities are listed in **Supplementary Figure 13g**.

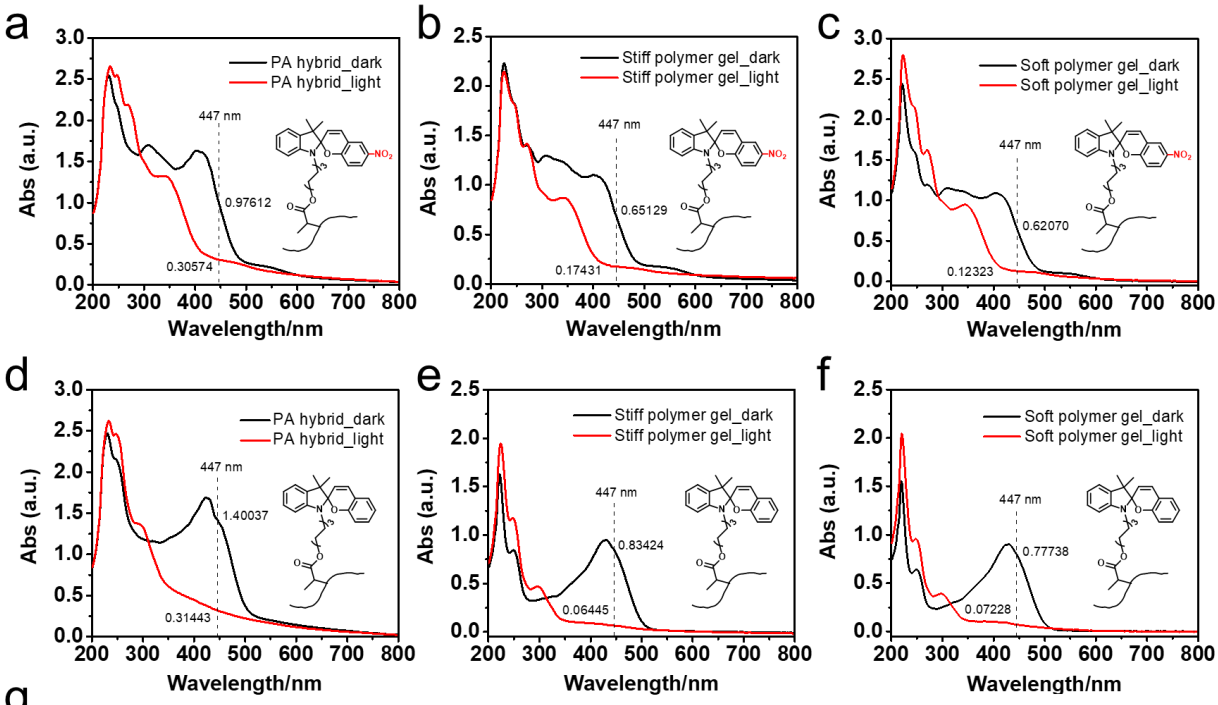

g

Spiropyrans / Hydrogel films	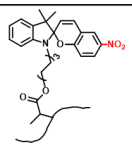		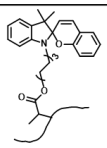	
	dark	light	dark	light
PA hybrid film	0.98	0.31	1.40	0.31
Stiff polymer film	0.65	0.17	0.83	0.06
Soft polymer film	0.62	0.12	0.78	0.07

Supplementary Figure 13 Calculation of optical density of hydrogel thin films (0.05 mm thick) with the swollen state in the dark and the shrunken state after light irradiation. **(a)** Plot of absorbance of PA hybrid hydrogel film containing nitro-spiropyran. **(b)** Plot of absorbance of stiff polymer hydrogel film containing nitro-spiropyran. **(c)** Plot of absorbance of soft polymer hydrogel film containing nitro-spiropyran. **(d)** Plot of absorbance of PA hybrid hydrogel film containing spiropyran without nitro substituent. **(e)** Plot of absorbance of stiff polymer hydrogel film containing spiropyran without nitro substituent. **(f)** Plot of absorbance of soft polymer hydrogel film containing spiropyran without nitro substituent. **(g)** Summary of optical densities of hydrogel thin films in the dark and in the light.

Light-induced mechanical reinforcement

A large piece (40 mm long × 30 mm wide) of hydrogel film (500 μm thick) was prepared according to the protocol above and left in the dark overnight. Disks with a diameter of 8 mm were produced using a puncher for rheology measurements on an Anton Paar Modular Compact Rheometer (MCR 302) in 8 mm parallel-plate geometry with a gap size of 0.4 mm. The rest of hydrogel film was exposed to a white LED for 1 h and punched followed immediately by measurement with the same testing parameters. Rheology measurements of PA hybrid hydrogels with variable amounts of the supramolecular PA components (0 wt%, 0.5 wt%, 1.0 wt%, 1.5 wt%) were carried out following the same protocol.

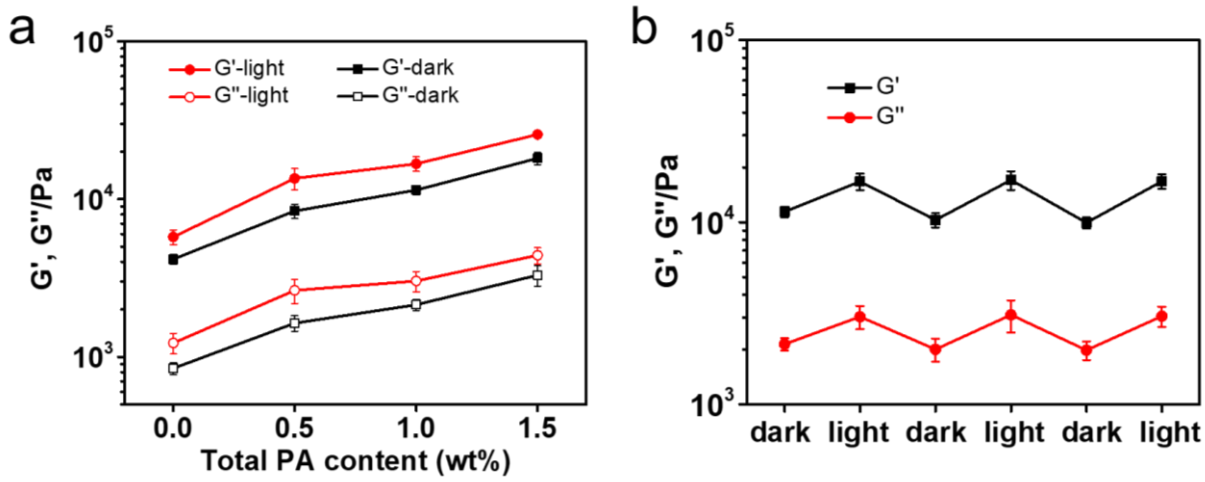

Supplementary Figure 14 (a) G' and G'' of the PA hybrid materials with different PA content before (black) and after (red) light irradiation. **(b)** G' and G'' of the PA (1 wt%) hybrid material by on and off irradiation over multiple cycles. Error bars represent standard deviations of data collected from three separate samples.

S4. Computational Methods

S4.1. All-atom simulations

We parametrized spiropyran, merocyanine and NIPAM using the general AMBER force field (GAFF)[12], according to the protocol in the Methods section (main text). DFT optimized geometries, atom types and partial charges are given below. A single polymer chain was assembled using 110:3 ratio of NIPAM to spiropyran (either SP or MC isomer) following the experimental molar ratios of monomers. This polymer chain was solvated with a TIP3P water model and equilibrated using the AMBER16[13] software with the following MD protocol. First, the system was minimized for 500 steps using the steepest descent method. Then, we gradually heated the system from 0 K to 100 K in 100 ps at constant volume (NVT). Next, we further increased the temperature from 100 K to 298 K in 100 ps at constant pressure (NPT) of 1 atm. After 10 ns of equilibration, we performed 300 ns of production simulation, which was used for gathering bond and angle distributions used in the coarse-grained model. For all simulations, a Langevin thermostat with a collision frequency of 2 ps^{-1} was used. For constant pressure simulations, we used the Berendsen thermostat with isotropic coupling.

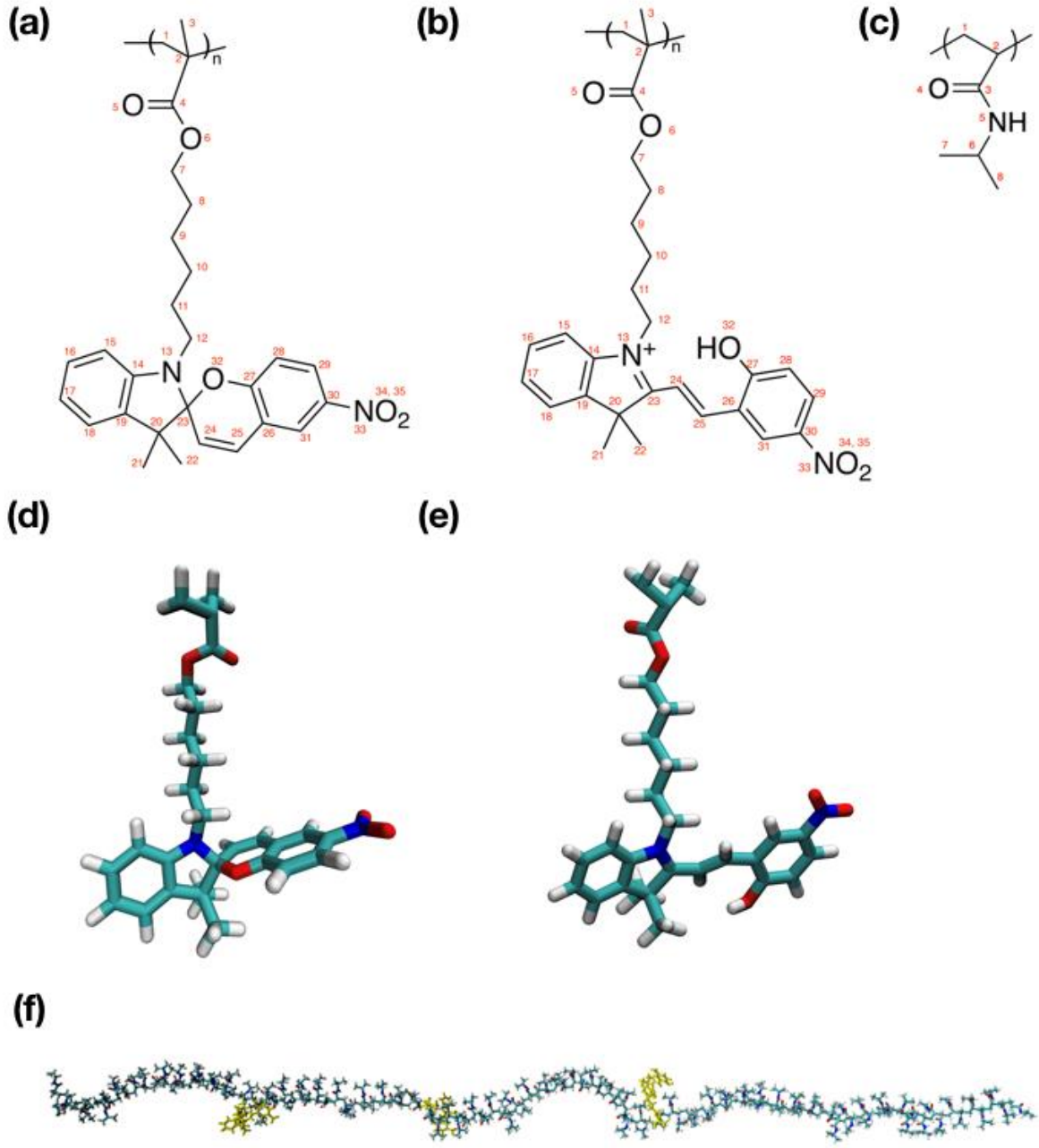

Supplementary Figure 15 Chemical structures of **(a)** spiropyran, **(b)** merocyanine and **(c)** NIPAM monomer with labels. DFT optimized structures of **(d)** spiropyran and **(e)** merocyanine. **(f)** Single copolymer chain with 110:3 molar ratio of NIPAM to spiropyran.

To build the components of our system, we first simulated the self-assembly of the PA nanofiber. Each peptide amphiphile consists of the amino acid sequence Val-Val-Val-Ala-Ala-Ala-Glu-Glu-Glu attached to a 16-carbon palmitoyl tail at the N-terminus. As in the experiments, the C-termini of PAs were amidated. Therefore, at neutral pH each PA chain has a net charge of –3.The initial structure for the seeded molecular dynamics simulation is constructed using the method in Lee et al.[1] by radially placing nine PA chains per layer and stacking 12 layers with a distance of 5 Å, resulting in a total of 108 PA chains for the complete structure. Visual Molecular Dynamics (VMD)[2] was used to solvate the structure with a TIP3P water model[3] in a box with dimensions 120 × 120 × 60 $Å^3$ in x, y and z, respectively. In addition, 0.15 M NaCl was added. We used CHARMM36 force field[4-6] for modeling the PA fiber in the self-assembly simulations. Molecular dynamics (MD) simulations were performed with NAMD 2.10 software[7]. Following a 1000 step minimization to remove high-energy contacts, the initial structures were equilibrated for 2 ns with a NPT ensemble at 310 K and 1 atm using the Langevin piston[8] Nose-Hoover method[9] implemented in NAMD. The damping coefficient was 5 ps^{-1} for temperature coupling using Langevin dynamics at 310 K. Pressure was kept at 1 atm with a Langevin piston period of 100 fs with a damping time constant of 50 fs. Full electrostatics was employed using the particle-mesh Ewald[10] method with a 1 Å grid width. Non-bonded interactions were calculated using a group-based cutoff with a switching function and updated every 10 time steps. Covalent bonds involving hydrogen were held rigid using the SHAKE algorithm[11], allowing a 2 fs time step. Atomic coordinates were saved every 10 ps for the trajectory analysis. Periodic boundary conditions were employed in x, y and z directions. In the production run, a 100 ns simulation was run using the same settings.

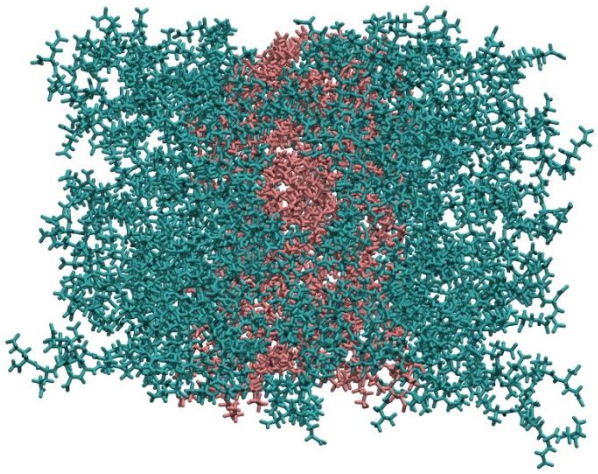

Supplementary Figure 16 Equilibrated all-atom PA nanofiber assembled from 108 $V_3A_3E_3$ PAs. The hydrophobic core of the PA is shown in pink while the peptide portion is shown in cyan.

Supplementary Table 1. Amber GAFF atom types and RESP partial charges for spiropyran (SP), merocyanine (MC) and NIPAM monomer shown in **Supplementary Fig. 15**.

Atom label	Atom type (SP)	RESP charge (SP)	Atom type (MC)	RESP charge (MC)	Atom type (NIPAM)	RESP charge (NIPAM)
1	c3	-0.1230	c3	-0.1368	c3	-0.0211
1-hydrogen[a]	hc	0.0106 (2)	hc	0.0169 (2)	hc	0.0417 (2)
2	c3	0.2510	c3	0.0866	c3	-0.1380
2-hydrogen	-	-	-	-	hc	0.0877 (1)
3	c3	-0.1307	c3	-0.1968	c	0.6611
3-hydrogen	hc	0.0339 (3)	hc	0.0591 (3)		-
4	c	0.4451	c	0.8106	o	-0.6141
5	o	-0.4960	o	-0.5557	n	-0.5719
5-hydrogen	-	-	-	-	hn	0.3065 (1)
6	os	-0.2481	os	-0.4584	c3	0.0967
6-hydrogen	-	-	-	-	hc	0.0897 (1)
7	c3	-0.3659	c3	0.0236	c3	-0.1101
7-hydgrogen	h1	0.1822 (2)	h1	0.0825 (2)	hc	0.0400 (3)
8	c3	0.0483	c3	0.0281	c3	-0.1101
8-hydgrogen	hc	0.0762 (2)	hc	0.0308 (2)	hc	0.0400 (3)
9	c3	-0.0574	c3	-0.0215		
9-hydrogen	hc	0.0166 (2)	hc	0.0107 (2)		
10	c3	0.0339	c3	0.0019		
10-hydrogen	hc	-0.014 (2)	hc	0.0157 (2)		
11	c3	0.0746	c3	-0.0082		
11-hydrogen	hc	0.0032 (2)	hc	0.0354 (2)		
12	c3	-0.1616	c3	-0.0742		
12-hydrogen	h1	0.0975 (2)	h1	0.0861 (2)		
13	na	-0.2443	na	0.0517		
14	ca	0.0901	ca	0.0162		
15	ca	-0.1424	ca	-0.1438		
15-hydrogen	ha	0.1373 (1)	ha	0.1700 (1)		
16	ca	-0.1759	ca	-0.1152		
16-hydrogen	ha	0.1287 (1)	ha	0.1505 (1)		
17	ca	-0.1094	ca	-0.0698		
17-hydrogen	ha	0.1146 (1)	ha	0.1452 (1)		
18	ca	-0.2227	ca	-0.1839		
18-hydrogen	ha	0.1425 (1)	ha	0.1639 (1)		
19	ca	0.0377	ca	0.0399		
20	c3	0.1788	c3	0.1443		
21	c3	-0.1633	c3	-0.1653		
21-hydrogen	hc	0.0441 (3)	hc	0.0678 (3)		
22	c3	-0.1633	c3	-0.1653		
22-hydrogen	hc	0.0441 (3)	hc	0.0678 (3)		
23	c3	0.1516	c2	0.1154		
24	c2	-0.0490	c2	-0.1920		
24-hydrogen	hc	0.1029 (1)	hc	0.1459 (1)		
25	c2	-0.2240	c2	-0.0513		
25-hydrogen	hc	0.1371 (1)	hc	0.1191 (1)		
26	ca	0.1179	ca	-0.0179		
27	ca	0.1515	ca	0.2447		
28	ca	-0.2163	ca	-0.1101		
28-hydogen	ha	0.1479 (1)	ha	0.1581 (1)		
29	ca	-0.0987	ca	-0.1315		
29-hydrogen	ha	0.1452 (1)	ha	0.1752 (1)		
30	ca	-0.0064	ca	0.0126		
31	ca	-0.1796	ca	-0.1296		
31-hydrogen	ha	0.1480 (1)	ha	0.1501 (1)		
32	os	-0.1561	oh	-0.4421		
32-hydrogen	-	-	ho	0.3663 (1)		
33	no	0.6129	no	0.6245		
34	o	-0.3859	o	-0.3478		
35	o	-0.3888	o	-0.3675		

[a]Numbers in parentheses next to hydrogens indicate the number of hydrogens bound to the carbon atom indicated by the atom label. All hydrogens bound to the same carbon have the same partial charge.

S4.2. Coarse-grained Model and Simulations

Coarse-grained model parametrization

We used the all-atom simulations of a single polymer chain with 110:3 NIPAM to SP/MC ratio to obtain the bonded parameters for our coarse-grained model. The bond and angle distributions calculated from all-atom simulations were compared with the ones from CG simulations. For these CG simulations, we constructed a single polymer chain in the same way as the all-atom simulations and performed MD simulations with the CG parameters until the distributions from all-atom simulations and CG simulations were in agreement. All coarse-grained simulations were performed using Gromacs 5.0.4 software[16] according to the following protocol. We first minimized for 5000 steps using steepest descent method. Then, we ran a constant volume (NVT) simulation for 1 ns using 10 fs time step at 298 K while the polymer chain was position restrained. In the second step of the equilibration, we ran a constant pressure (NPT) simulation with 20 fs time step for 20 ns at 298 K and 1 bar pressure. Following the equilibration, we performed a production run for 500 ns using NPT ensemble with 20 fs time step. The compressibility for the pressure coupling was 3×10^{-4} bar^{-1}. The cutoff for Lennard–Jones potential was 12 Å and the LJ potential was smoothly shifted to zero between 9 Å and 12 Å. The cutoff used for Coulombic potential was also 12 Å. For electrostatic interactions, we used the group method with dielectric constant 2.5, which is appropriate for polarizable MARTINI water model. For LJ potential a group cutoff was used. The neighbor list was updated every 10 steps. MARTINI constraints were handled using the LINCS algorithm.[17] Parameters given in **Supplementary Tables 2 and 3** for CG mapping given were used for the simulations. We used the MARTINI polarizable water model[18] to solvate our polymer and added counter ions (Cl^-) to neutralize the charges for MCH^+-PNIPAM simulations. Bond and angle distributions were obtained from the 500 ns production run and the parameters in **Supplementary Table 3** were optimized according to the distributions from all-atom simulations. **Supplementary Fig. 18** shows the comparison of the distributions for the parameters given in **Supplementary Table 3**. We see that most of the bonded parameters are in agreement while there are some that differ between the all-atom and coarse-grained simulations. The disagreement in some bond lengths arises because of the limitations of the CG structure. The all-atom structure, especially the bonds in the rings of spiropyran, are more flexible and compact while they are constrained to protect the stability of the structure in the CG model. However, we believe this small difference in bond length distributions is not significant and does not affect the behavior of our model.

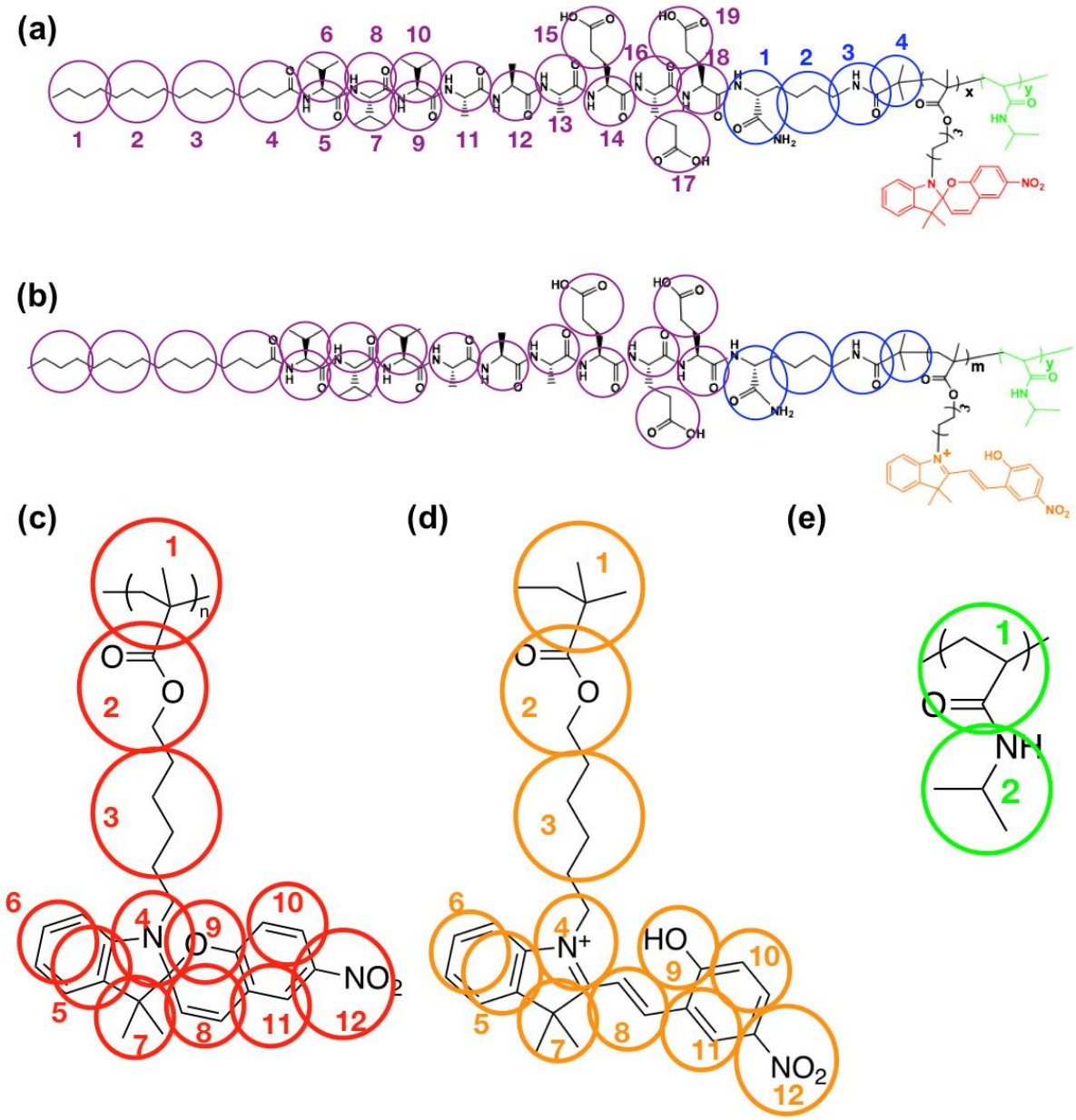

Supplementary Figure 17 Coarse-grained (MARTINI) mapping for the **(a)** PA-SP chain **(b)** PA-MCH$^+$ chain **(c)** spiropyran (SP), **(d)** merocyanine (MCH$^+$) and **(e)** NIPAM with bead labels. $V_3A_3E_3$ PA is shown in purple. The initiator that links PA to polymer is shown in blue. Two isomers of spiropyran are shown in red (SP) and orange (MCH$^+$). NIPAM monomer is shown in green.

Supplementary Table 2. Coarse-grained mapping of spiropyran and merocyanine. See **Supplementary Fig. 17** for the chemical structures.

BEAD	PA MARTINI Bead Label (Type)	Initiator MARTINI Bead Label (Type)	SP MARTINI Bead Label (Type)	MCH^+ MARTINI Bead Label (Type)	NIPAM MARTINI Bead Label (Type)
1	T1 (C1)	I1 (P5)	BB (C1)	BB (C1)	BB (Na)
2	T2 (C1)	I2 (C3)	SP1(Na)	MC1 (Na)	PSC (Nd)
3	T3 (C1)	I3 (P3)	SP2 (C1)	MC2 (C1)	
4	T4 (Na)	I4 (C2)	SP3 (SN0)	MC3 (SQ0)	
5	BB (P5)		SP4 (SC5)	MC4 (SC5)	
6	SC1 (C2)		SP5 (SC5)	MC5 (SC5)	
7	BB (Nda)		SP6 (C1)	MC6 (C1)	
8	SC1 (C2)		SP7 (SC4)	MC7 (SC4)	
9	BB (Nda)		SP8 (SN0)	MC8 (SP1)	
10	SC1 (C2)		SP9 (SC4)	MC9 (SC4)	
11	BB (P4)		SP10 (SC4)	MC10 (SC4)	
12	BB (P4)		SP11(Na)	MC11 (Na)	
13	BB (P4)				
14	BB (P5)				
15	SC1 (P1)				
16	BB (P5)				
17	SC1 (P1)				
18	BB (P5)				
19	SC1 (P1)				

Supplementary Table 3. Optimized bonded parameters for coarse-grained model of spiropyran (SP), merocyanine (MCH^+), initiator and PNIPAM. See previous work[14]and MARTINI force field[15] for the PA parameters.

Molecule	Bonds	function	R_{bond} (nm)	K_{bond} (kJ mol^{-1} nm^{-2})	Angles	function	θ_0 (deg)	K_{angle} (kJ mol^{-1})	dihedrals	function	Φ_{pd}	K_{pd} (kJ mol^{-1})
SP	BB-SP1	1	0.288	10000					SP5-SP3-SP6-SP4	2	0.0	50
	SP1-SP2	1	0.385	2000					SP7-SP8-SP9-SP10	2	0.0	50
	SP2-SP3	1	0.385	2000								
	SP3-SP7	1	0.282	7000								
	SP3-SP8	1	0.262	7000								
	SP7-SP10	1	0.244	10000								
	SP8-SP9	1	0.252	10000								
	SP9-SP11	1	0.318	10000								
	SP10-SP11	1	0.312	10000								
	SP3-SP4	1	0.284	constraint								
	SP4-SP5	1	0.192	constraint								
	SP4-SP6	1	0.244	constraint								
	SP3-SP6	1	0.328	constraint								
	SP7-SP8	1	0.248	constraint								
	SP9-SP10	1	0.254	constraint								
MCH^+	BB-MC1	1	0.298	10000					MC5-MC3-MC6-MC4	2	0.0	50
	MC1-MC2	1	0.385	2000								
	MC2-MC3	1	0.385	2000								
	MC3-MC7	1	0.462	2000								
	MC9-MC11	1	0.316	10000								
	MC10-MC11	1	0.280	10000								
	MC3-MC4	1	0.332	constraint								
	MC4-MC5	1	0.216	constraint								
	MC4-MC6	1	0.234	constraint								
	MC3-MC6	1	0.310	constraint								
	MC7-MC10	1	0.221	constraint								
	MC9-MC10	1	0.254	constraint								
	MC8-MC9	1	0.252	constraint								
	MC8-MC10	1	0.256	constraint								
NIPAM	BB-PSC	1	0.332	5000	BB-BB-PSC	1	107	20				
Initiator	BB-I1	1	0.350	1250	I1-I2-I3	2	180	25				
	I1-I2	1	0.330	5000	I2-I3-I4	2	180	25				
	I2-I3	1	0.280	5000								
	I2-I4	1	0.322	5000								
	I4-BB	1	0.349	5000								
Polymer backbone	BB-BB	1	0.349	5000	BB-BB-BB	1	98	100				

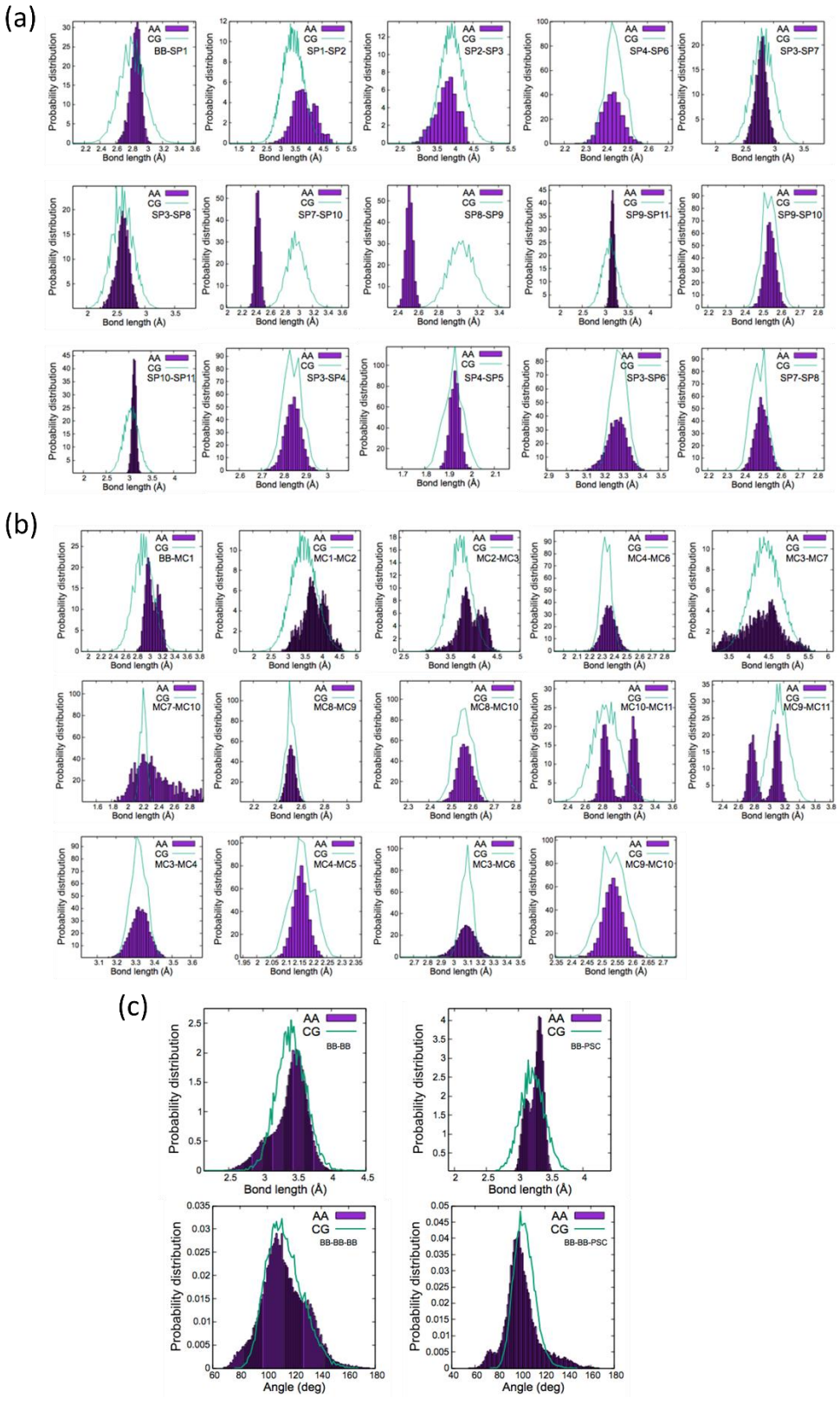

Supplementary Figure 18 Bond and angle distributions from all-atom and coarse-grained simulations for **(a)** spiropyran (SP) **(b)** merocyanine (MCH^+) and **(c)** PNIPAM.

To validate our nonbonded parameters (MARTINI bead types given in **Supplementary Table 2**), we calculated free energy of solvation in water and octanol for spiropyran (SP) and NIPAM monomer using all-atom simulations. The results of these simulations were compared to the ones obtained using the CG model. All atom simulations were performed using Amber GAFF force field parameters given in **Supplementary Table 1** for spiropyran and NIPAM monomer. Octanol parameters derived for GAFF using a similar procedure was taken from Calemen et al.[19] and the TIP3P water model was used. For the free energy of hydration, ΔG_w, a single monomer of spiropyran was placed in a box filled with water. For the free energy of solvation in octanol, ΔG_o, a single monomer of spiropyran was placed in a box filled with octanol and water in the ratio 199:66. The interaction between solute and solvent was decoupled first using 11 λ values (0, 0.1, 0.2, …, 1) for electrostatic interaction, followed by 11 λ values (0, 0.1, 0.2, ..,1) for Lennard–Jones interactions. This procedure was repeated by running separate simulations in water and octanol phases for NIPAM monomer. All TI calculations were performed using Gromacs 5.0.4 software.[16] Before running TI simulations, each box was minimized for 5000 steps using steepest descent method and then equilibrated for 10 ns with 2 fs time step using an NPT ensemble at 298 K and 1 bar pressure. Periodic boundary conditions were applied in all directions. The temperature was maintained at 298 K using a velocity-rescaling thermostat with coupling constant of 1.0 ps. For constant pressure simulations (NPT), isotropic pressure coupling was applied using a Berendsen thermostat with a coupling constant of 5.0 ps. The compressibility for the pressure coupling was 4.5×10^{-5} bar^{-1}. Verlet cutoff scheme was used for neighbor search. The cutoff for Lennard–Jones potential and Coulombic potential was 12 Å. For electrostatic interactions, we used the PME method. After the equilibration, TI simulations were carried for 6 ns at each λ value using the same settings.

The same procedure was repeated for the coarse-grained structures. All of the solutes were represented with the parameters developed using the MARTINI force field given in **Supplementary Tables 2** and **3**. Force field parameters for octanol were taken from the MARTINI force field. Polarizable water model[18] was used for water. Because the coarse-grained spiropyran and NIPAM do not have any charged beads, only LJ interaction was decoupled using 11 λ values (0, 0.1, 0.2, …, 1). Prior to TI calculations, each solute was minimized for 5000 steps and equilibrated for 50 ns with 20 fs time step using an NPT ensemble at 298 K and 1 bar pressure. The compressibility for the pressure coupling was 3×10^{-4} bar^{-1} The cutoff for Lennard-Jones potential was 12 Å and the LJ potential was smoothly shifted to zero between 9 Å and 12 Å. The cutoff used for Coulombic potential was also 12 Å. For electrostatic interactions, we used the group method with dielectric constant 2.5, which is appropriate for polarizable MARTINI water model. For LJ potential a group cutoff was used. The neighbor list was updated every 10 steps. MARTINI constraints were handled using the LINCS algorithm.[17] After the equilibration, TI simulations were carried for 10 ns at each λ value using the same settings.

Supplementary Table 4 below shows the free energy of solvation values calculated for spiropyran and PNIPAM monomer in water and octanol phases as well as the octanol–water partition coefficient (P_{ow}). It should be noted that TI calculations were performed only for the spiropyran (SP) isomer since it is not difficult to assign the charged bead type in the MC isomer.

Supplementary Table 4. Free energy of hydration, ΔG_W, free energy of solvation, ΔG_o, free energy change between water and octanol phases, $\Delta\Delta G_{ow}$, and partition coefficient, $\log P_{ow}$, obtained from TI calculations.

Solute	ΔG_o (kJ/mol)	ΔG_w (kJ/mol)	$\Delta\Delta G_{ow}$ (kJ/mol)	$\log P_{ow}$
All-atom SP	-146.17 ± 0.52	-79.28 ± 0.50	-66.89	11.72
Coarse-grained SP	-145.1 ± 0.40	-77.85 ± 0.45	-67.25	11.79
All-atom NIPAM	-40.91 ± 1.61	-31.33 ± 0.07	-9.58	1.68
Coarse-grained NIPAM	-29.52 ± 0.08	-24.75 ± 0.10	-4.77	0.84

PA-polymer hybrid simulations

After parametrization of our coarse-grained model, we built a hybrid PA-polymer structure, shown in **Supplementary Fig. 19.** To construct this structure, we first mapped our equilibrated PA fiber (**Supplementary Fig. 16**) to the CG model. Consistent with the experiments, 50% of the PAs (54/108) in this structure was polymerized by attaching the polymer chain with ratio 110:3 NIPAM to spiropyran through a linker molecule (**Supplementary Fig. 17**) in the extended conformation. Because these experiments were performed in acidic pH conditions, we protonated the GLU residues in the PA. The initial size of the box was 63 x 63 x 5.6 nm^3. We used the Martini polarizable water model[18] to solvate our hybrid structures and added counter ions (Cl^-) to neutralize the charges for MCH^+-PNIPAM simulations. The initial structures are shown in **Supplementary Fig. 19**. All coarse-grained simulations were performed according to the following protocol. We first minimized for 1000 steps using steepest descent method. Then, we ran a constant volume (NVT) simulation for 1 ns using 10 fs time step at 298 K while only PA molecules were position restrained. There were no position restraints on the polymer chains. In the second step of the equilibration, we ran a constant pressure (NPT) simulation with 20 fs time step for 20 ns at 298 K and 1 bar pressure with no position restraints. Following the equilibration, we performed a production run for 5 µs using NPT ensemble with 20 fs time step. The compressibility for the pressure coupling was $3x10^{-4}$ bar^{-1}. The cutoff for Lennard-Jones potential was 12 Å and the LJ potential was smoothly shifted to zero between 9 Å and 12 Å. The cutoff used for Coulombic potential was also 12 Å. For electrostatic interactions, we used the group method with dielectric constant 2.5, which is appropriate for polarizable Martini water model. For LJ potential a group cutoff was used. The neighbor list was updated every 10 steps. Martini constraints were handled using the LINCS algorithm.[17] Parameters given in **Supplementary Tables 2** and **3** were used for the simulations. We also assembled simulations were two fibers were in contact (**Supplementary Fig. 21**) in a box with initial size of 100 x 63 x 5.6 nm^3. After solvating the box with polarizable water and ions, the same procedure was used as above but these simulations were performed for 10 µs during the production step. Finally, we also constructed systems with no PA fiber, consisting of only 54 polymer chains (110:3 NIPAM to spiropyran ratio) randomly distributed in a box of initial size 30 x 30 x 30 nm^3 (**Supplementary Fig. 22**). The box was solvated with polarizable water and neutralized with ions. These simulations were performed for 5 µs using the same procedure as above. For all three systems (hybrid PA-polymer fiber, 2

hybrid PA-polymer fibers and polymer only), both light (SP) and dark (MCH^+) conditions were simulated separately.

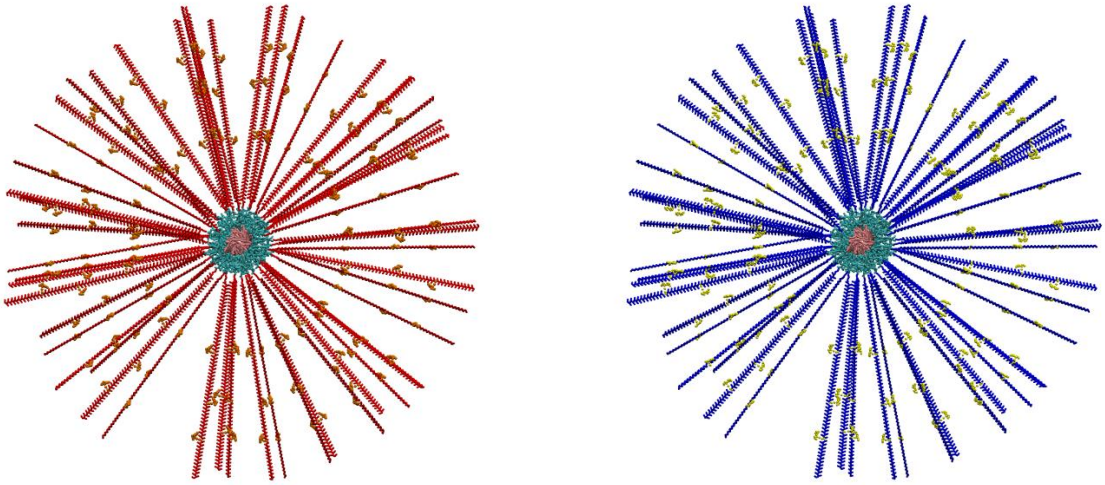

Supplementary Figure 19 Top view of initial conformations of hybrid polymer experiments with PA nanofiber using SP-PNIPAM (red) and MCH^+-PNIPAM (blue). The hydrophobic core of PAs is colored in pink, the peptide sequence is colored in cyan. Water and ions are omitted for clarity. SP isomers are colored in orange while MCH^+ isomers are colored in yellow.

.

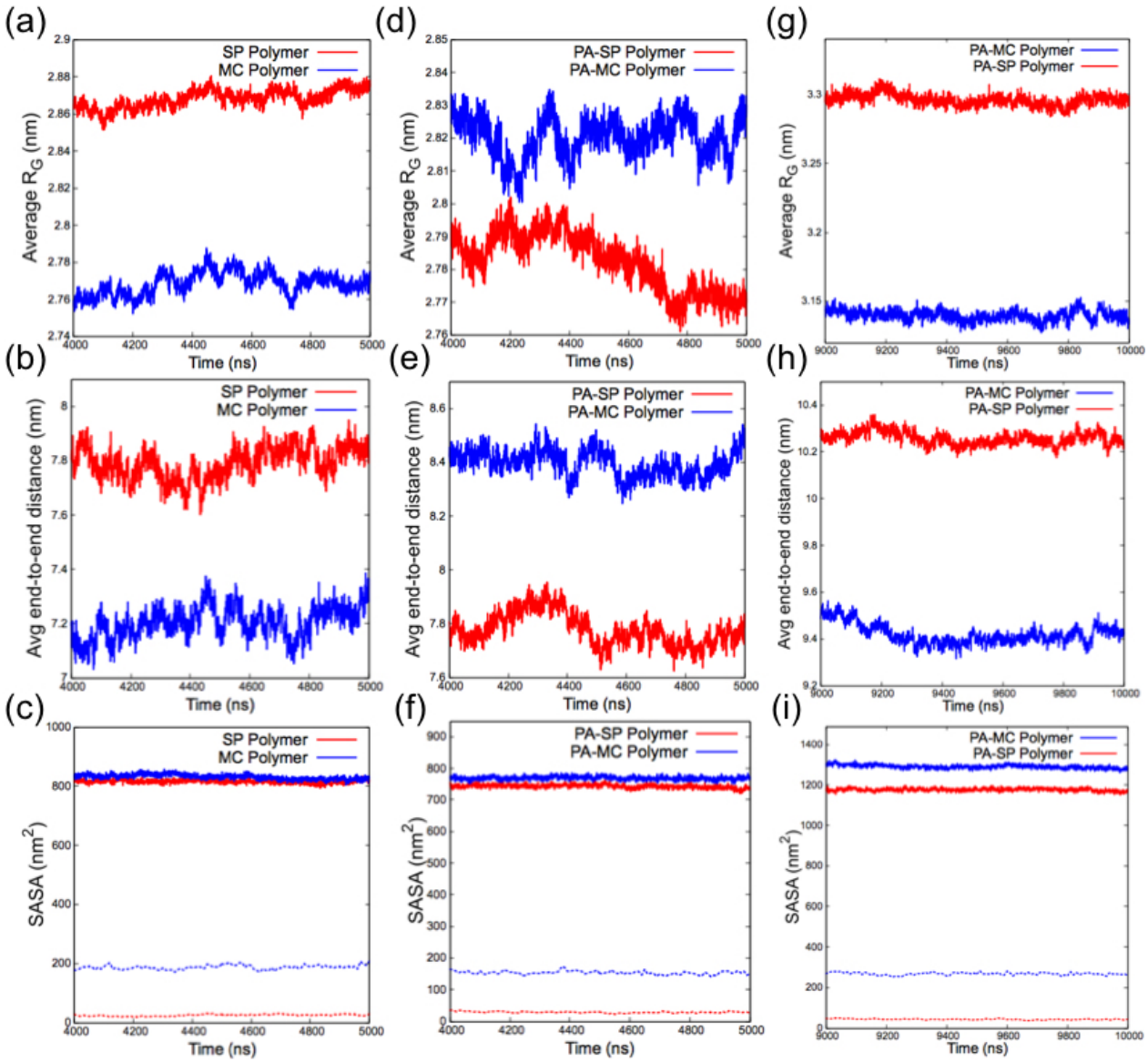

Supplementary Figure 20 Change in average (**a**, **d**, **g**) radius of gyration (**b**, **e**, **h**) end-to-end distance and (**c**, **f**, **i**) solvent accessible surface area (SASA) of individual polymer chains for control polymer, hybrid polymer and interacting hybrid polymer systems, respectively, over the last 1 μs of simulation time. Radius of gyration and end-to-end distance are calculated as averages of all chains in the system at each timestep. SASA is calculated for the polymer chains (solid line) and spiropyran molecules (dashed line).

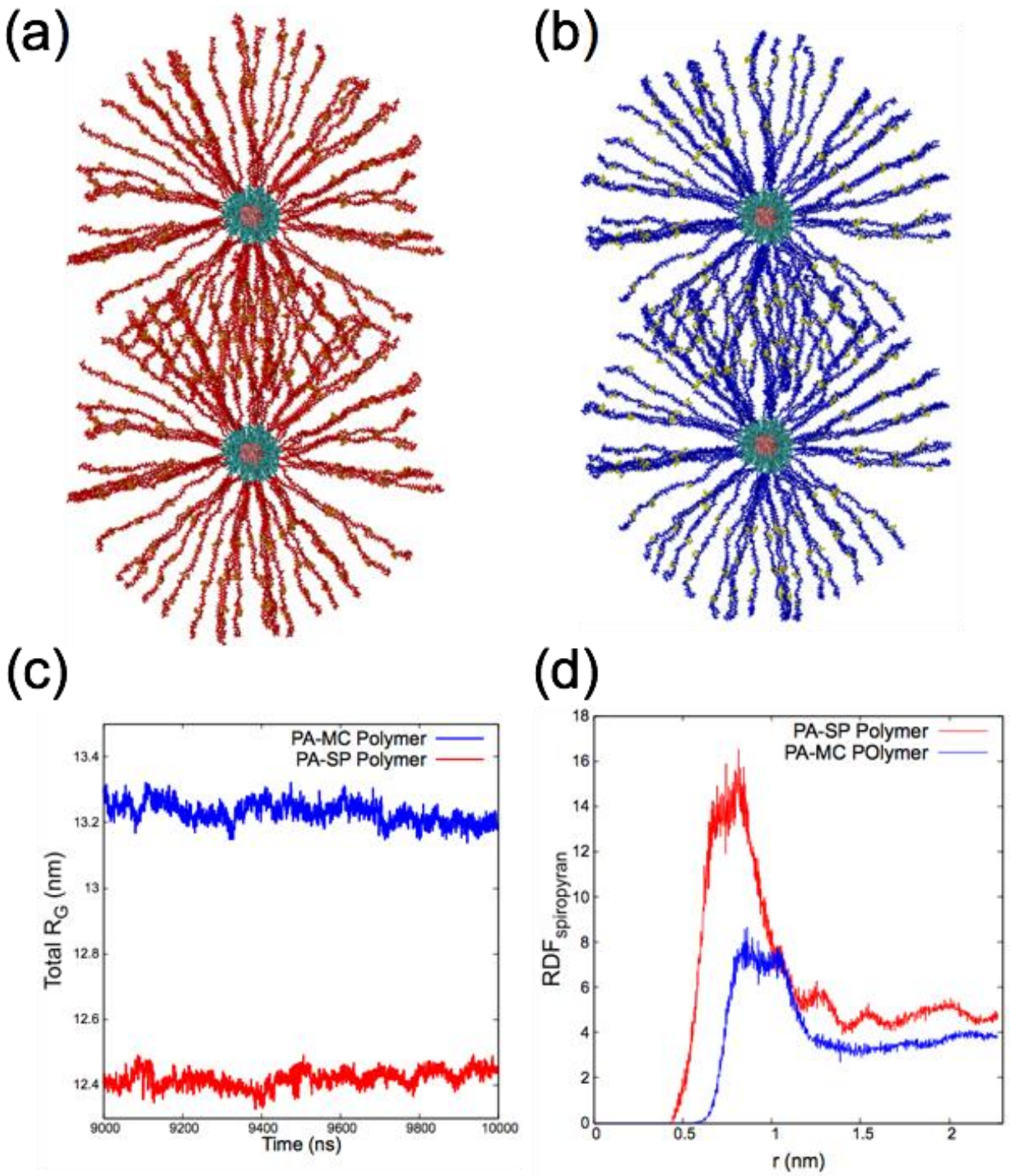

Supplementary Figure 21 Top views of initial conformations of interacting hybrid polymer experiments with two PA nanofibers using **(a)** SP-PNIPAM and **(b)** MCH^+-PNIPAM (blue). The hydrophobic core of PAs is colored in pink and the peptide sequence is colored in cyan. Water and ions are omitted for clarity. SP isomers are colored in orange while MCH^+ isomers are colored in yellow. **(c)** Total radius of gyration for the hybrid polymer system. **(d)** Radial distribution function for the spiropyran molecules calculated using the SP3/MC3 bead in each spiropyran molecule averaged over the last 500 ns of each simulation.

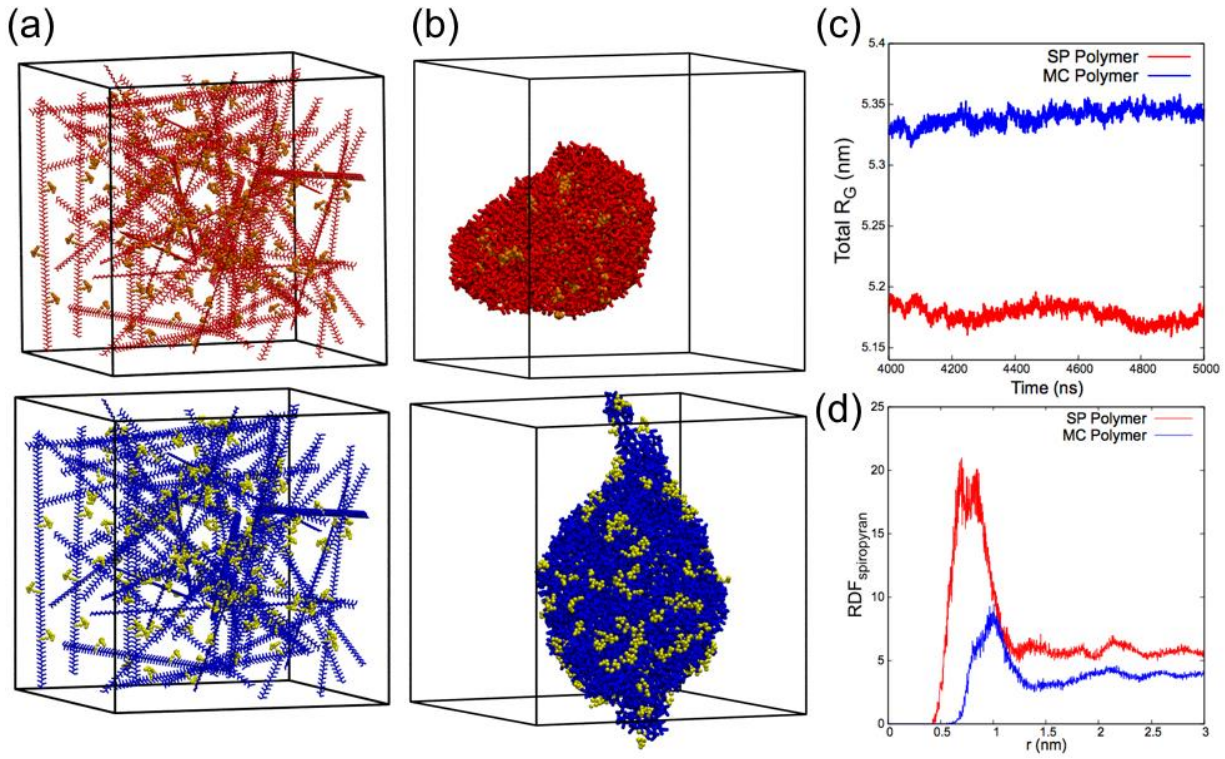

Supplementary Figure 22 Snapshots of **(a)** initial and **(b)** final conformations at 5 μs of control experiments with no PA nanofiber using SP-PNIPAM (red) and MCH^+-PNIPAM (blue). Water and ions are omitted for clarity. SP isomers are colored in orange while MCH^+ isomers are colored in yellow. **(c)** Total radius of gyration for the spiropyran-polymer only system. **(d)** Radial distribution function for the spiropyran molecules calculated using the SP3/MC3 bead in each spiropyran molecule averaged over the last 500 ns of each simulation.

Targeted MD simulations

To obtain the different conformations along our reaction coordinate (total radius of gyration, R_G) for the PMF calculation, we ran a Targeted Molecular Dynamics (TMD) simulation for the control and hybrid polymer systems. For both systems, we simulated the contraction process (MC → SP) using the equilibrated structures from our 5 μs MD simulations. All of the TMD simulations were performed using NAMD 2.10 software[7] with settings for MARTINI force field. MARTINI specific parameters such as the cosine-based angle potential function and Lennard–Jones switching were turned on, and the dielectric constant was set to 15.0. Electrostatic interactions were calculated with a cutoff of 12 Å. The LJ potential was smoothly shifted to zero between 9 Å and 12 Å. Following a 1000 step minimization to remove high-energy contacts, a 50 ns with a NPT ensemble at 298 K and 1 atm using the Langevin piston[8] Nose–Hoover method[9] implemented in NAMD. The damping coefficient was 1 ps^{-1} for temperature coupling using Langevin dynamics at 298 K. Pressure was kept at 1 atm with a Langevin piston period of 2000 fs with a damping time constant of 1000 fs. The time step was set to 20 fs. The TMD simulation was performed starting from the equilibrated MC structure to reach the equilibrated SP structure as target. The force constant for the TMD was 400 kcal/mol $Å^2$. Atomic coordinates were saved every 100 ps for the trajectory analysis. Periodic boundary conditions were employed in x, y and z directions.

Umbrella sampling and PMF calculation

We chose the total radius of gyration as the reaction coordinate for our umbrella sampling simulations. For the control polymer system, the R_G range from 5.1 nm (SP-PNIPAM) to 5.35 nm (MCH^+-PNIPAM) was divided into 11 windows with 0.025 nm intervals. For the hybrid polymer system, the R_G range from 7.45 nm (PA-SP-PNIPAM) to 7.9 nm (PA-MCH^+-PNIPAM) was divided into 19 windows with 0.025 nm intervals. The constraint on R_G at the center of each window in the umbrella sampling was achieved by a harmonic potential with a force constant of 300 kcal/mol. Each umbrella sampling window was simulated for 30 ns using the same settings as TMD simulations. The first 10 ns of each umbrella sampling window was discarded as equilibration. The potential mean force was calculated using the weighted histogram analysis method (WHAM)[20] using the distributions obtained from the umbrella sampling simulations. The number of bins used for the WHAM calculation was 125 and the tolerance was set to 0.00001 for convergence.

Supplementary Table 5. Change in fiber cross section (diameter, eccentricity and linear PA density) for different systems calculated from the last 500 ns of each simulation.

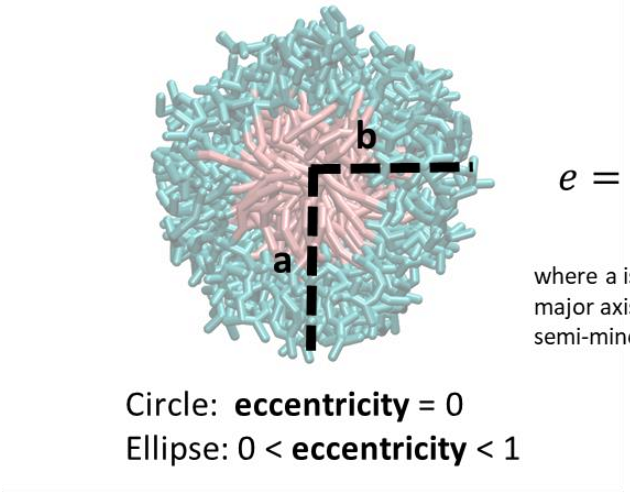

Systems	Fiber diameter (nm)	Fiber eccentricity	Linear PA density (PA/nm)
PA fiber only	5.88 ± 0.09	0.231 ± 0.07	19.2 ± 0.01
PA-SP polymer	6.42 ± 0.04	0.576 ± 0.02	20.9 ± 0.003
PA-MCH^+ polymer	6.38 ± 0.02	0.315 ± 0.03	21.6 ± 0.003

Results from Second Set of Simulations

In order to increase the statistical accuracy and show the reproducibility of our simulations, we repeated the coarse-grained MD simulations with and without the PA fiber starting from the initial structures in **Supplementary Figure 19** and **22a.** These simulations were performed using the exact same procedure and model but with different initial randomized velocities. Therefore, the results obtained are completely independent of the first set of simulations.

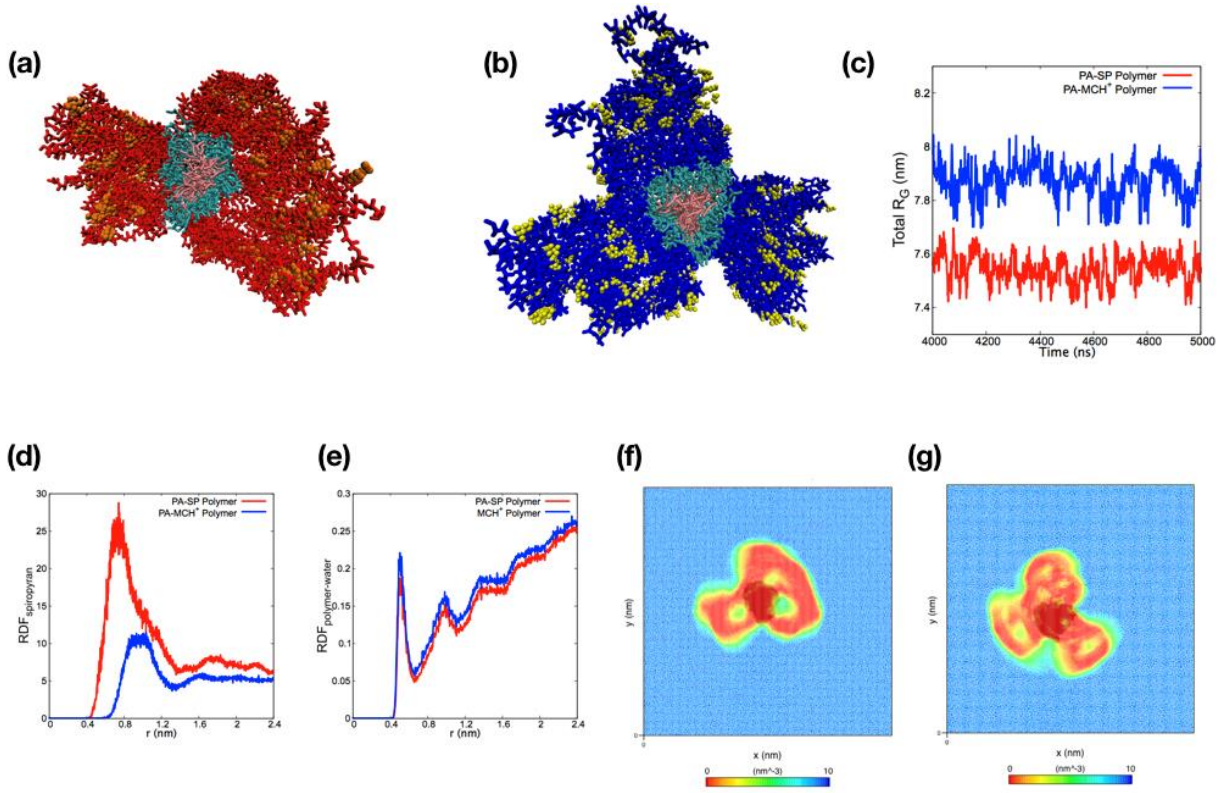

Supplementary Figure 23 Results of 2nd set of simulations for hybrid polymer in light (SP) and dark (MCH^+) conditions. Snapshots of final conformations at 5 μs of PA hybrid polymer experiments with single PA nanofiber using **(a)** SP-PNIPAM (red) and **(b)** MCH+-PNIPAM (blue). The hydrophobic core of the PAs is colored in pink, the peptide sequence is colored in cyan. Water and ions are omitted for clarity. SP isomers are colored in orange while MCH+ isomers are colored in yellow. **(c)** Total radius of gyration for the PA hybrid polymer system. **(d)** Radial distribution function (RDF) for the spiropyran molecules calculated using the SP3/MC3 bead in each spiropyran molecule averaged over the last 500 ns of each simulation. **(e)** RDF between the polymer and water molecules averaged over the last 500 ns of each simulation. 2D spatial distribution of water number density averaged over z and last 250 ns of simulation time for **(f)** PA-SP polymer and **(g)** PA-MCH+ polymer. The shaded region in the center shows the position of the PA fiber as a 2D density distribution calculated in the same manner.

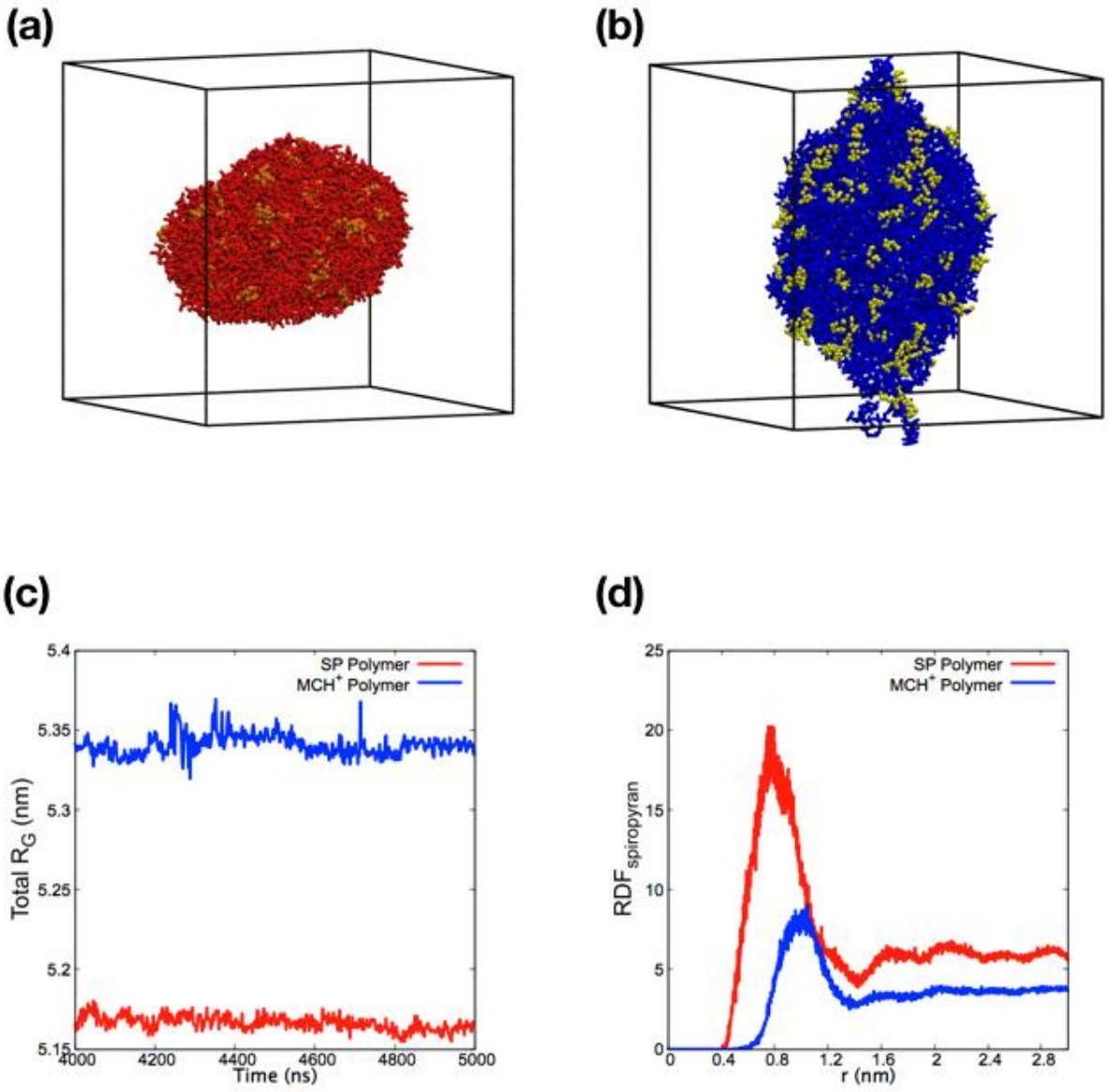

Supplementary Figure 24 Snapshots of final conformations at 5 μs of control experiments with no PA nanofiber using **(a)** SP-PNIPAM (red) and **(b)** MCH^+-PNIPAM (blue). Water and ions are omitted for clarity. SP isomers are colored in orange while MCH^+ isomers are colored in yellow. **(c)** Total radius of gyration for the spiropyran-polymer only system. **(d)** Radial distribution function for the spiropyran molecules calculated using the SP3/MC3 bead in each spiropyran molecule averaged over the last 500 ns of each simulation.

S5. Characterization of photoactuation behaviors

Bending angle normalization

Even though the total number of photoactive (MCH^++SP) units is the same, the hybrid material obviously contains supramolecular polymer not present in the covalent network, thus the weight fraction of photoactive units is lower when the supramolecular component is present. The bending angle was normalized based on the weight fraction of photoactive units, taking into account the fact that the ratio of total polymer (including covalent network and supramolecular polymer) to photoswitch moieties is constant.

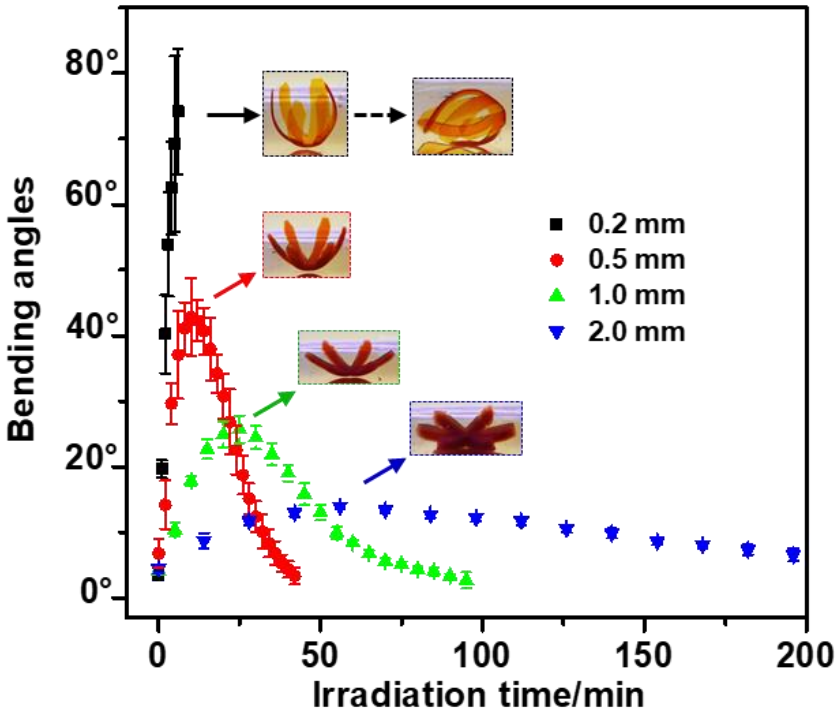

Supplementary Figure 25 Bending angles of hydrogel flower films with variable thickness from 0.2 mm to 2 mm were measured by ImageJ over different irradiation times. Error bars represent standard deviations of data collected from three separate samples.

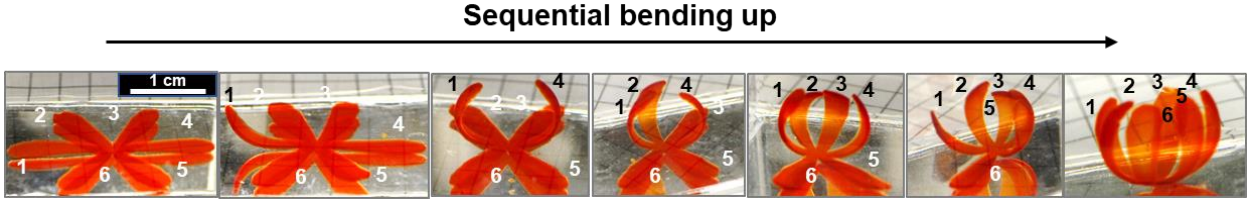

Supplementary Figure 26 Sequential bending of a flower-shaped hybrid film was shown by local irradiation at specific petals, labeled 1 through 6.

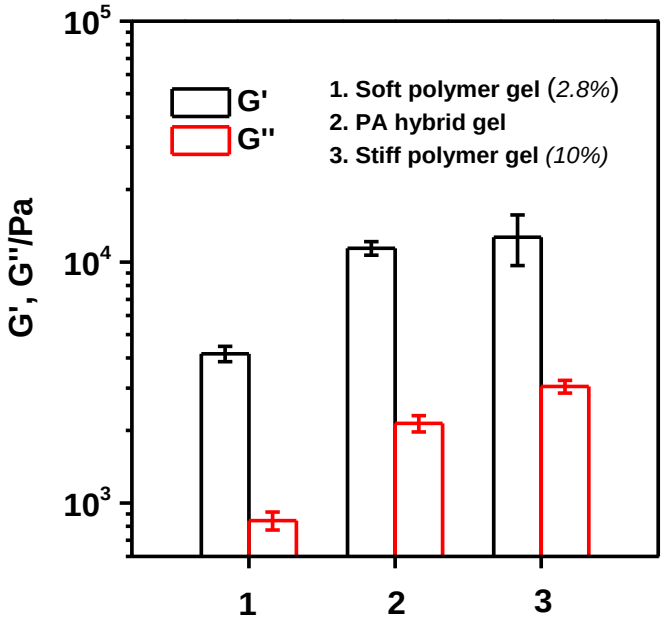

Supplementary Figure 27 Rheological study of polymer hydrogels with different crosslinker densities compared to the PA hybrid hydrogel. Error bars represent standard deviations of data collected from three separate samples.

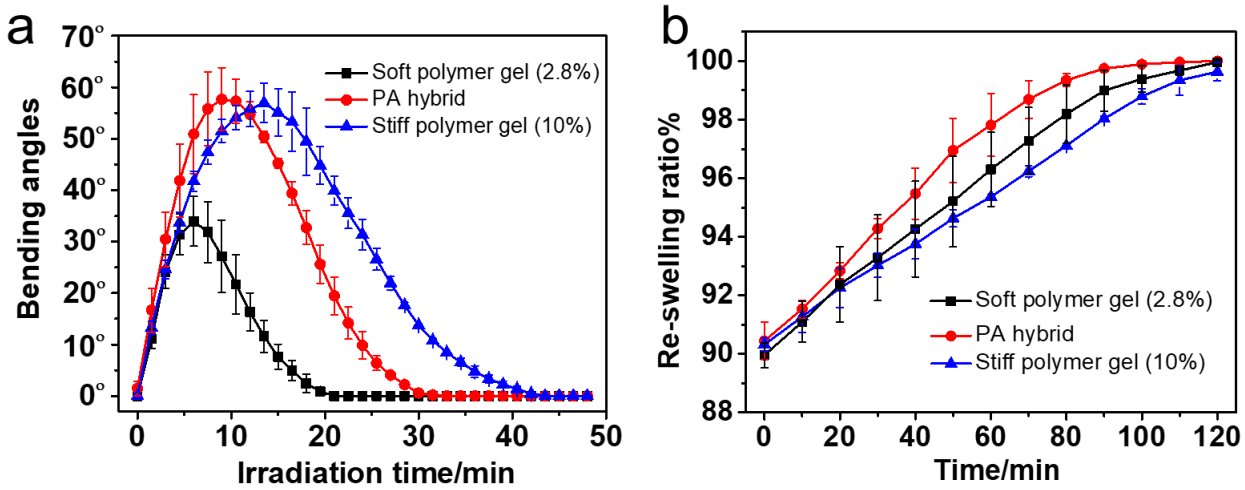

Supplementary Figure 28 (a) Bending kinetics of PA hybrid films made of a spiropyran molecule without the nitro substituent compared to polymer films with different crosslinker densities (2.8% or 10%). **(b)** Re-swelling kinetics in the dark of PA hybrid films made of a spiropyran molecule without the nitro substituent compared to soft or stiff polymer films. Error bars represent standard deviations of data collected from three separate samples.

Ring-opening rate in the dark

Spontaneous ring-opening kinetics in the dark was studied by measuring the recovery of maximum absorbance at 414 nm for nitro-spiropyran and 430 nm for spiropyran without the nitro substituent.

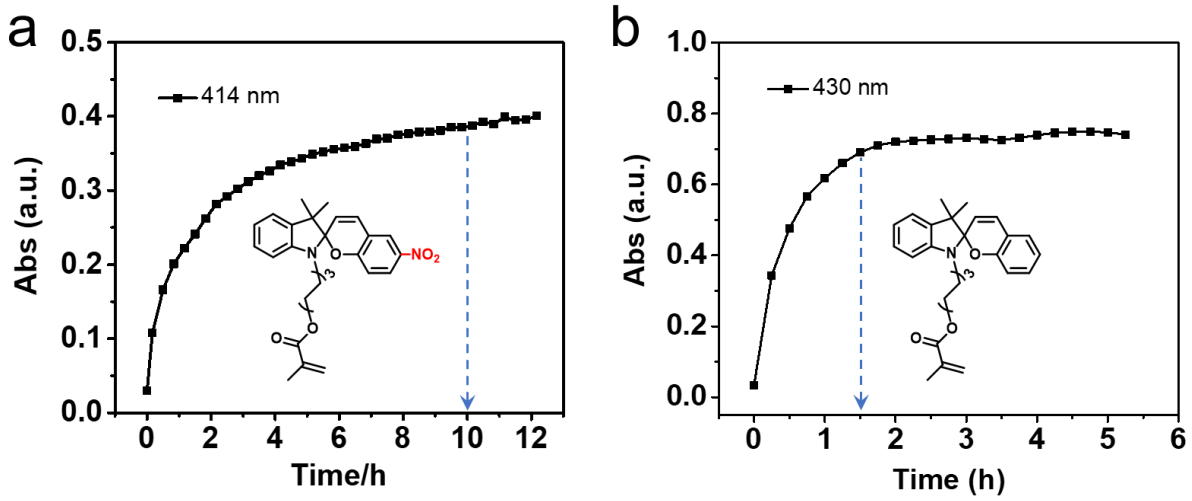

Supplementary Figure 29 (a) Time-dependent absorbance recovery in the dark of the nitro-spiropyran molecule (**3a**, 0.1 mM) in methanol/water (4/1, v/v) containing 5 mM HCl. **(b)** Time-dependent absorbance recovery in the dark of the spiropyran molecule without the nitro substituent (**3b**, 0.1 mM) in methanol/water (4:1, v/v) containing 5 mM HCl.

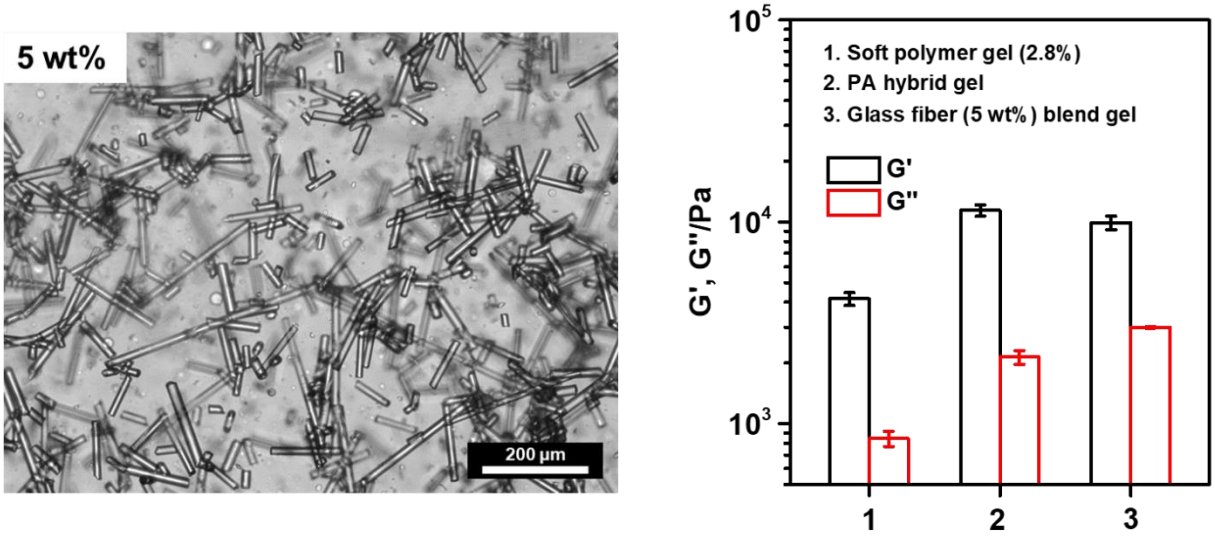

Supplementary Figure 30 Left, optical microscopic image of glass fiber (5 wt%) blended polymer hydrogel (2.8% of crosslinker). Right, mechanical reinforcement by physically adding glass fiber (5 wt%) into the polymer hydrogel. Error bars represent standard deviations of data collected from three separate samples.

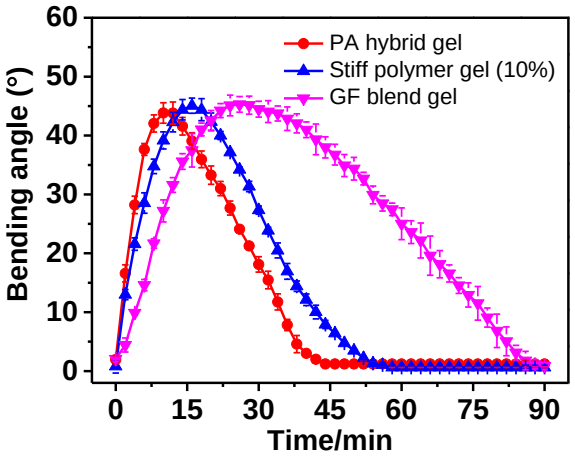

Supplementary Figure 31 Actuation kinetics for polymer hydrogels when blended with non-photoactive glass fiber (5 wt%) compared to stiff polymer gel and PA (1 wt%) hybrid gel. Error bars represent standard deviations of data collected from three separate samples.

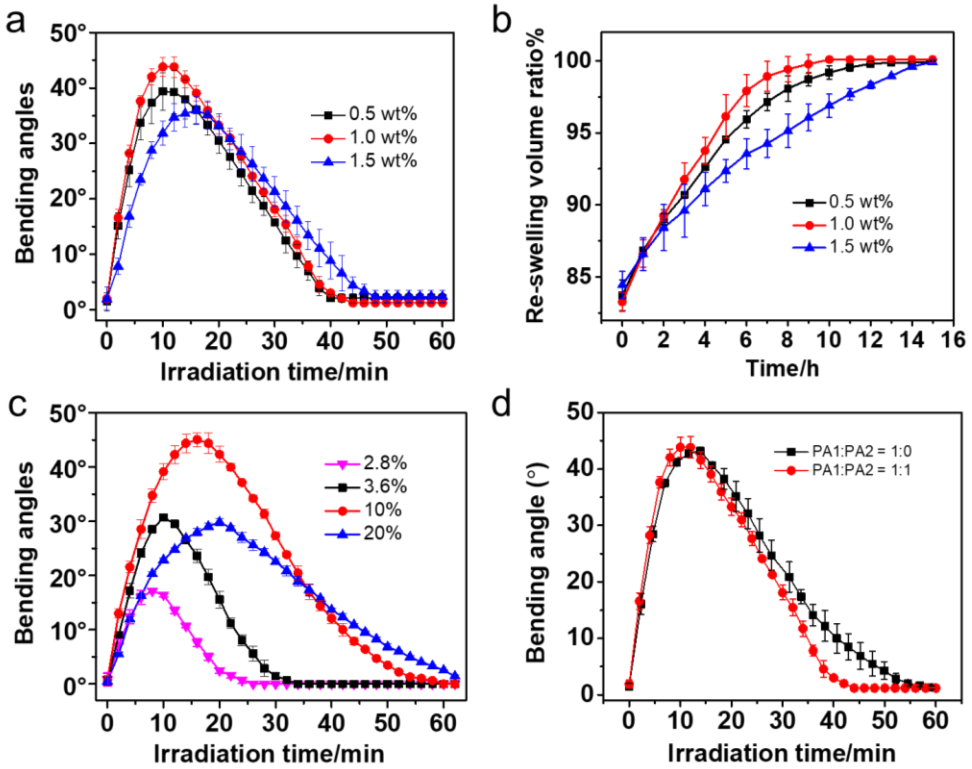

Supplementary Figure 32 Photoactuation kinetics of PA hybrid hydrogels made of nitro-spiropyran by varying PA content while keeping the weight fraction of covalent polymer constant at 10 wt%. **(a)** Light-induced bending kinetics of PA hybrid hydrogels containing different weight fractions of the supramolecular component. **(b)** Reswelling kinetics in the dark of the PA hybrid hydrogels containing different weight fractions of the supramolecular component. **(c)** Bending kinetics of covalent hydrogel with different crosslinking densities. (**d**) Bending kinetics of PA (1 wt%) hybrid hydrogel made of 100 mol% of PA1 + 0 mol% of PA2 (black) compared to 50 mol% of PA1 + 50 mol% of PA2 (red). Error bars represent standard deviations of data collected from three separate samples.

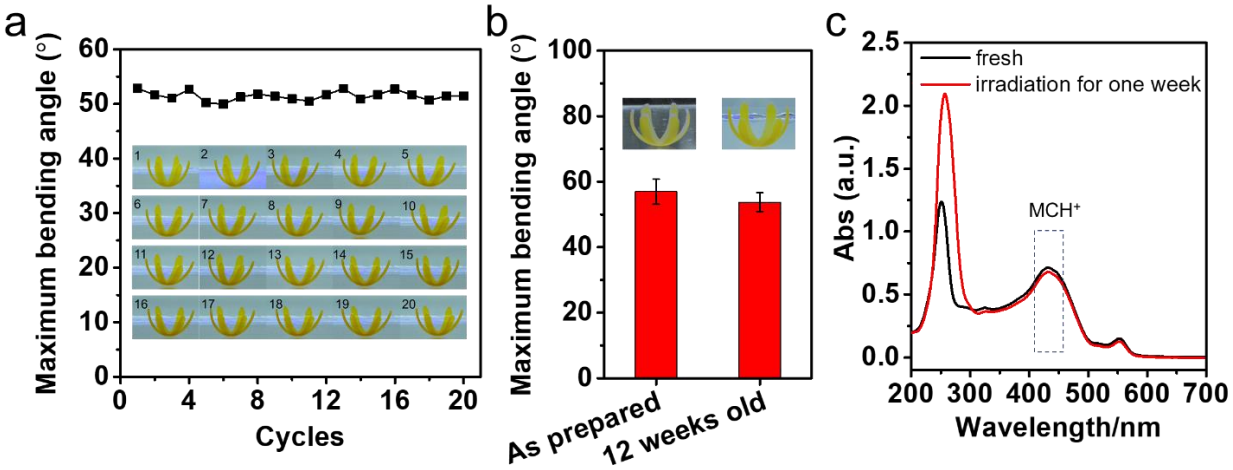

Supplementary Figure 33 Robustness of PA hybrid hydrogels containing spiropyran moiety without nitro substituent. **(a)** Plot of the maximum bending angle of a hydrogel flower over 20 cycles of bending and flattening by switching the light source on and off. For each cycle, the light and dark period takes 40 min and 2 h, respectively. Inset shows photographs of the flower with the maximum bending angle for each cycle. **(b)** Plot of the maximum bending angles of a hydrogel flower as prepared and stored in acidic water (5 mM HCl) for 12 weeks. Error bars represent standard deviations of data collected from three separate samples. **(c)** UV-Vis spectra of spiropyran molecule without nitro substituent (0.1 mM) in dioxane/water solvent (4/1, v/v) containing 5 mM HCl. Black, freshly prepared sample; red, the same sample after irradiation light (447 nm, 0.3 mW/cm^2) for one week and recovery overnight in the dark.

3D printing

Monomers of *N*-isopropylacrylamide (NIPAAm, 500 mg, 4.42 mmol), methacrylate-spiropyran (45.2 mg, 95.2 μmol) and methacrylate-PA/filler PA (1:1 molar ratio , 50 mg, 40.5 μmol), and crosslinker N,N-methylenebisacrylamide (MBAAm, 19.0 mg, 123.5 μmol) were dissolved in dioxane/water (4:1 v/v, 5 mL) in a 15 mL tube. This solution was annealed following the same protocol for hydrogel preparation above and photoinitiator diphenyl(2,4,6-trimethylbenzoyl) phosphine oxide photoinitiator (25.0 mg, 71.8 μmol) was added. This stock solution was pre-photopolymerized for 40 s by putting the solution between a pair of 100-watt white light LEDS (Chanzon, 6000-6500K color temperature, Amazon ASIN B01DBZHUXA) to get a partially polymerized soft gel as the printing ink. This ink was extruded through a 0.25 mm inner diameter nozzle (Nordson EFD) into 3 cm × 3 cm squares on glass substrates using an EnvisionTEC 3D-Bioplotter System. The tip-to-substrate distance was 250 μm, with a print speed of 10 mm s^{-1} and an extrusion pressure between 2 and 3 bar. The printed gel was ~500 μm thick consisting of two printed layers. After printing, the gels were placed in a 500 μm thick glass mold and stock solution (NIPAAm/PA/methacrylate-spiropyran/MBAAm/photoinitiator) was added to fill the gap between printed filaments, followed by a secondary photopolymerization to get the final printed squares. These squares were cut into either a flower shape or crawler shape according to the patterns used above. In our bilayer structures, the filament orientation between the first and second layer is perpendicular to each other for flower bending kinetics study, or parallel to each other for crawling motion study. As a control, a sample without alignment (random sample) was prepared by casting the soft gel ink into a glass mold with thickness of 500 μm followed by the secondary polymerization.

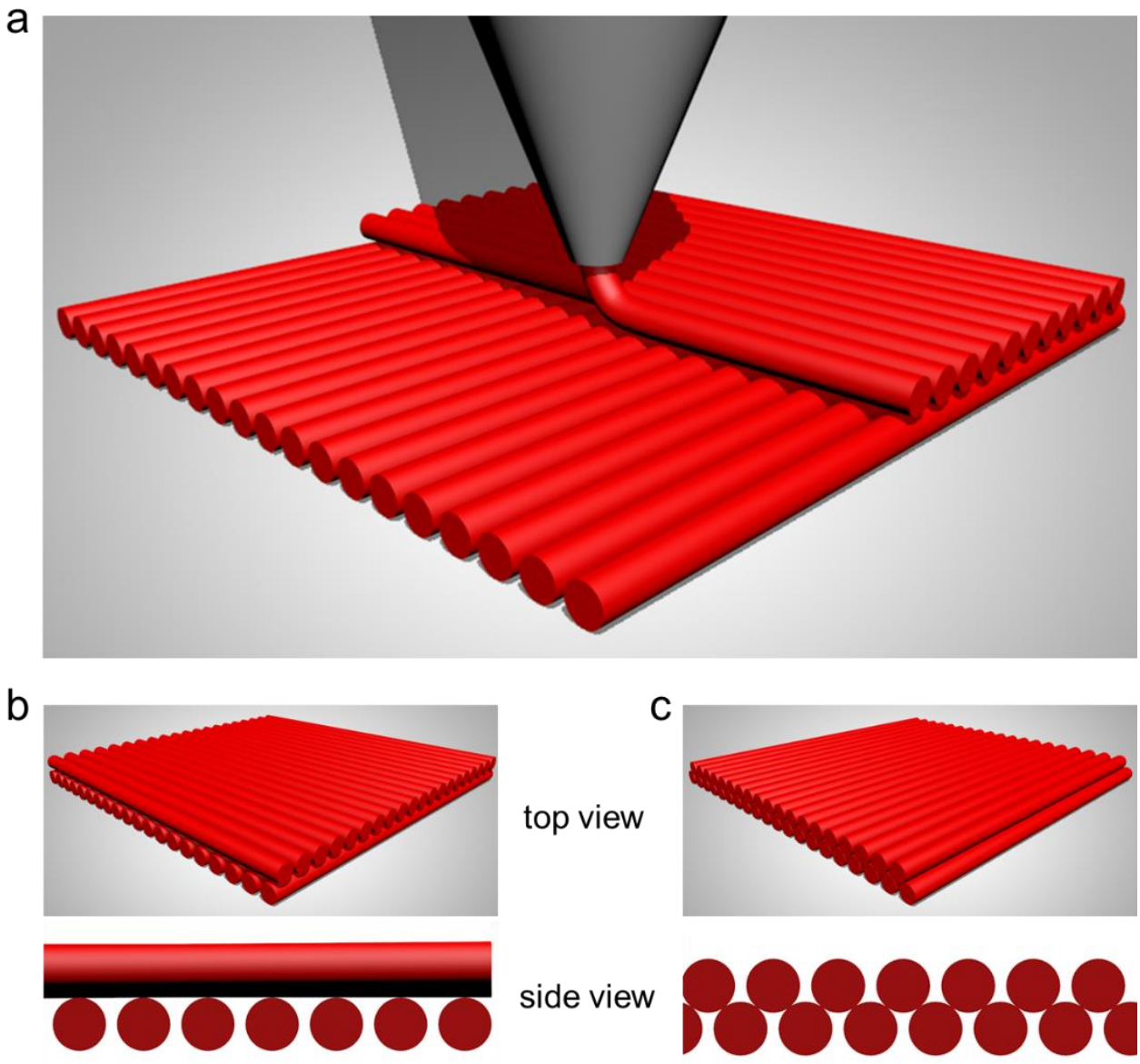

Supplementary Figure 34 (a) Schematic representation of extrusion printing PA hybrid materials. **(b)** Schematic representation of the printing process for PA hybrid materials as a two-layer thick film (500 µm total thickness) with a perpendicular orientation of printed filaments. **(c)** Schematic representation of the printing process for PA hybrid materials as a two-layer think film (500 µm thick in total) with a parallel orientation of printed filaments.

Polarized optical microscopy

The printed thin films before the secondary polymerization were imaged in between two perpendicular light polarizers using a Leica DM750 P instrument in reflection mode with a 4× magnification using Leica Application Suite V4.2 software. The sample stage allowed for the precise rotation and *x*, *y*-positioning of the samples. Images were recorded with sample oriented at 0° and 45° with respect to the polarizer.

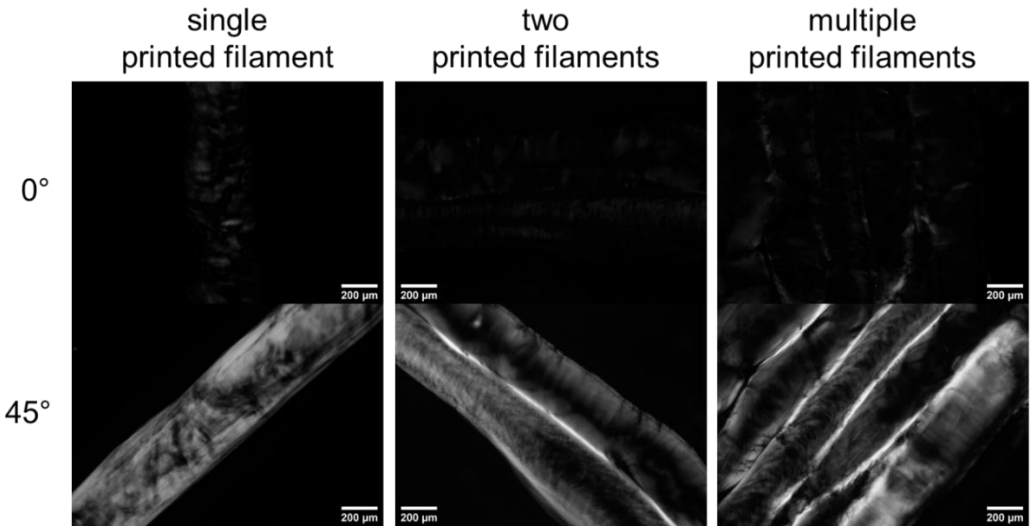

Supplementary Figure 35 Polarized optical micrographs of printed filaments of PA hybrid material. Images were recorded with samples at 0° (top) and 45° (bottom) relative to the polarizer and increasing numbers of filaments from left to right.

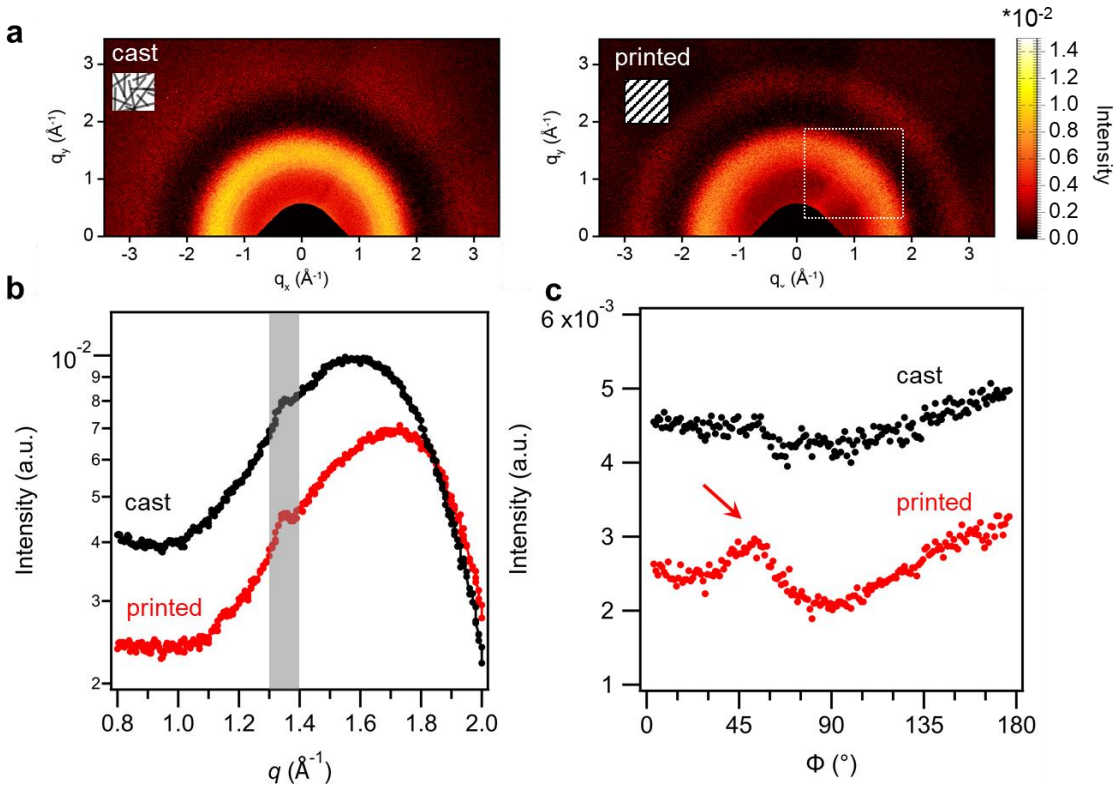

Supplementary Figure 36 (a) 2D WAXS patterns of cast (top) and printed (bottom) PA-PNIPAM hybrid hydrogels. Note: the printed gels are oriented with the extrusion direction ~45° to the detector as represented schematically by the inset. **(b)** 1D integrated line cuts of cast (black) and printed (red) gels showing the presence of a β-sheet peak at 1.35 Å^{-1} in both samples from the PA fibers. **(c)** Azimuthal line cuts for 1.3 Å^{-1} < q < 1.4 Å^{-1} showing preferential alignment of the β-sheet peak in the extrusion direction for the printed sample.

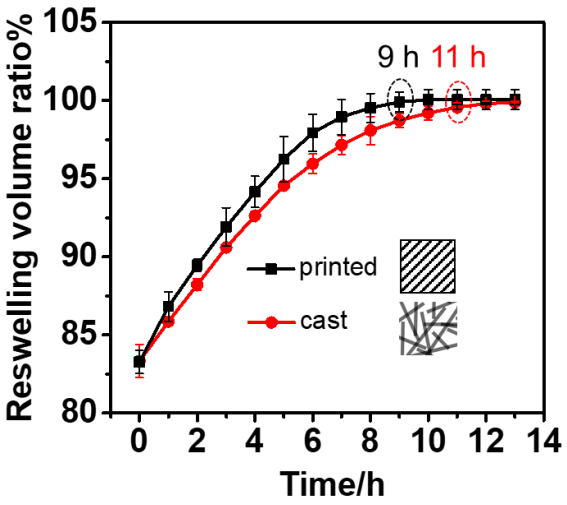

Supplementary Figure 37 Reswelling kinetics of 3D printed (aligned, black) and cast (non-aligned, red) PA (1 wt%) hybrid films made of nitro-spiropyran in the dark. Error bars represent standard deviations of data collected from three separate samples.

S6. Characterization of crawling motion on ratcheted surface

Ratcheted surface preparation

Plastic ratcheted molds with different grooves were 3D printed and these ratcheted patterns were transferred to PDMS by adding processors to the plastic molds followed by thermal curing. PDMS ratcheted surface with 2.0 mm spacing and 1.43 mm high, or 0.7 mm spacing and 0.5 mm high were made following this protocol.

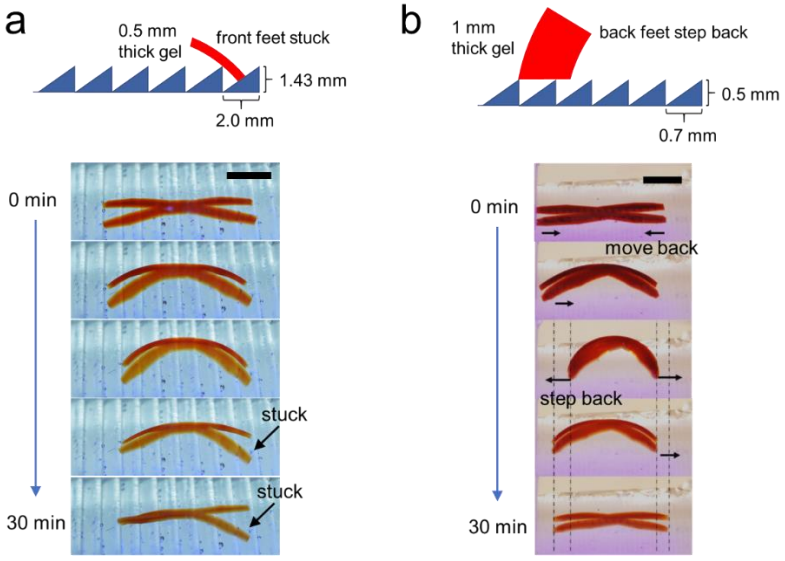

Supplementary Figure 38 Mismatch in the size of the ratchet spacing and crawler thickness failed to drive the unidirectional crawling motion from left to right. **(a)** 2 mm surface spacing caused the crawler feet to get stuck at the groove. **(b)** The ratcheted surface cannot control the motion direction if the gel thickness (1.0 mm) is bigger than ratchet spacing (0.7 mm).

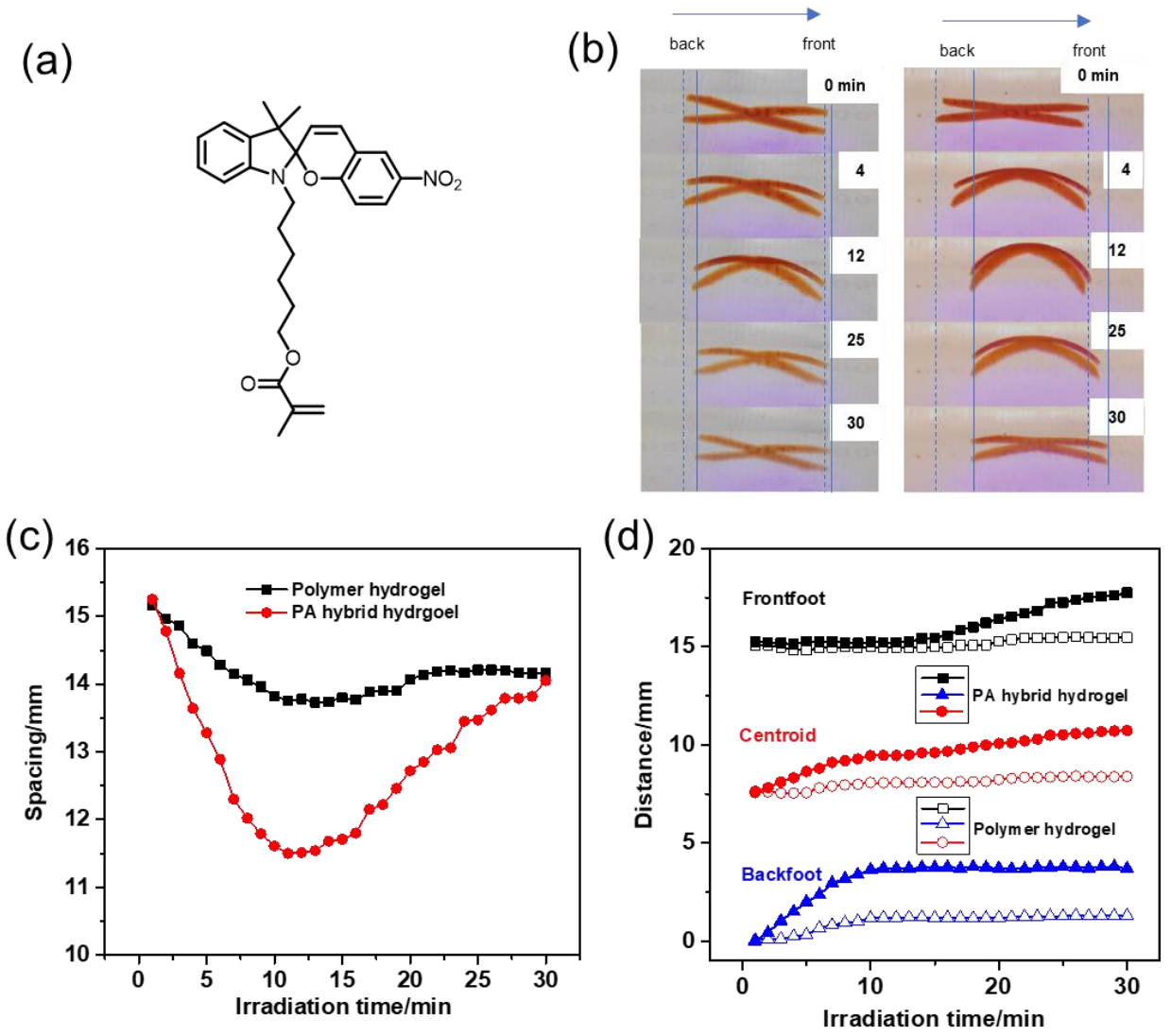

Supplementary Figure 39 (a) Chemical structure of nitro-spiropyran**.** (**b**) Snapshots of the actuator at variable walking time. Left, polymer hydrogel (2.8%); right, PA hybrid hydrogel. The spacing between the front foot and back foot are shown in (**c**) and the positions of front foot, back foot as well as the centroid are shown in (**d**).

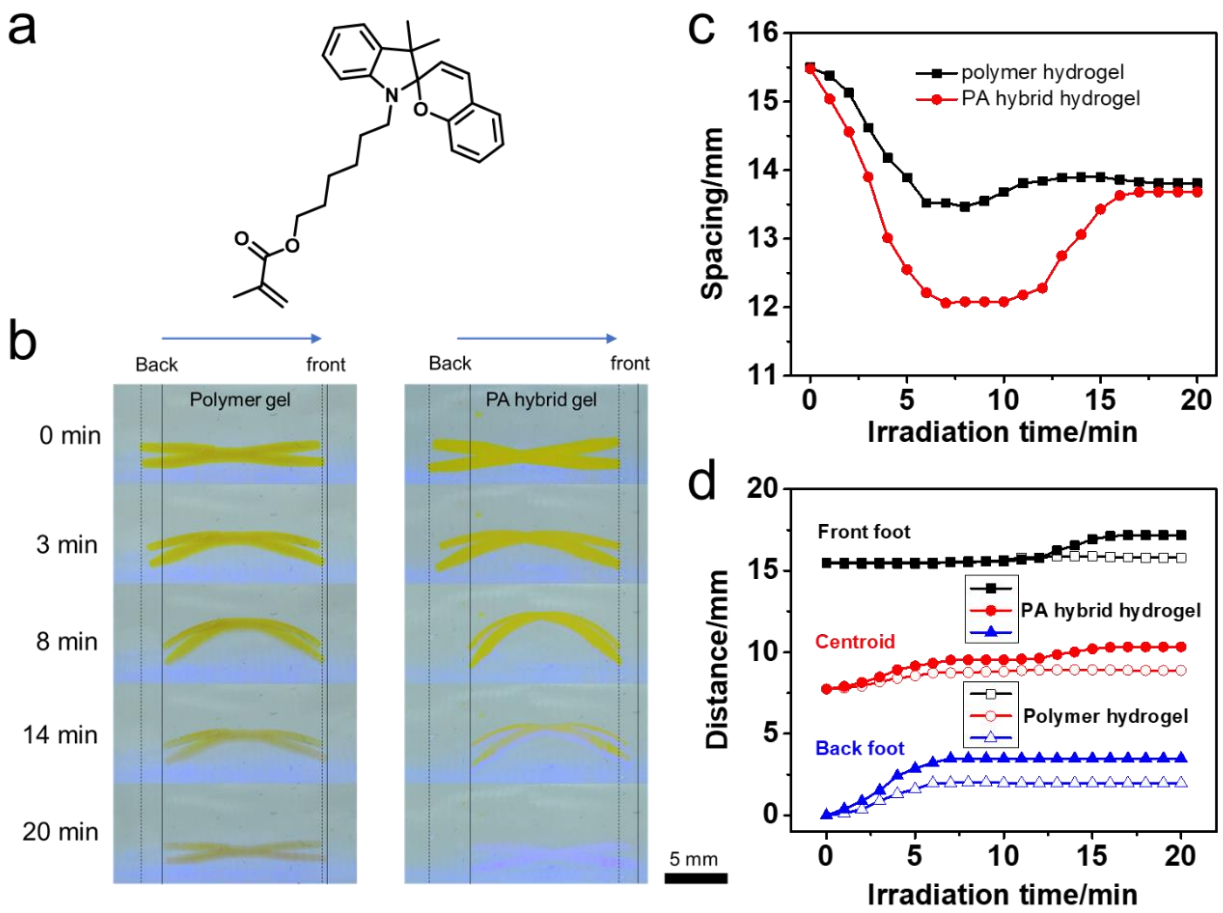

Supplementary Figure 40 (a) Chemical structure of a spiropyran molecule without the nitro substituent. **(b)** Photographs of PA hybrid crawler on the ratcheted surface moving unidirectionally from left to right. Left, covalent polymer crawler; right, PA hybrid crawler. **(c)** Plotting of spacing between front back feet and **(d)** distance of front feet, back feet as well as centroid vs irradiation time.

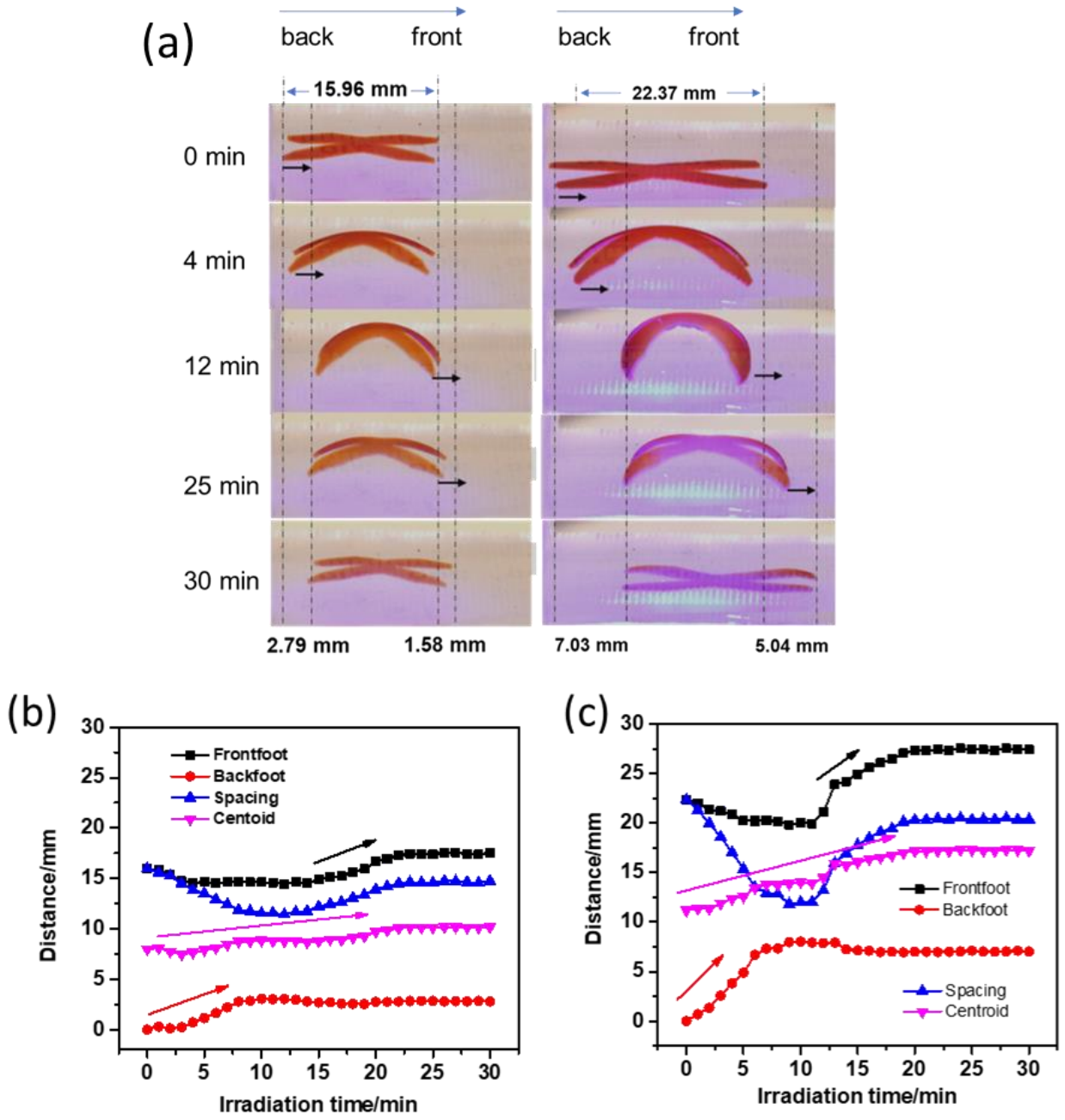

Supplementary Figure 41 (a) Snapshots comparing PA hybrid hydrogel actuators that are 16 mm (left) or 22 mm (right) long. The spacing between the front foot and back foot, the positions of front foot, back foot as well as the centroid are shown for **(b)** the 16 mm walker and **(c)** the 22 mm walker.

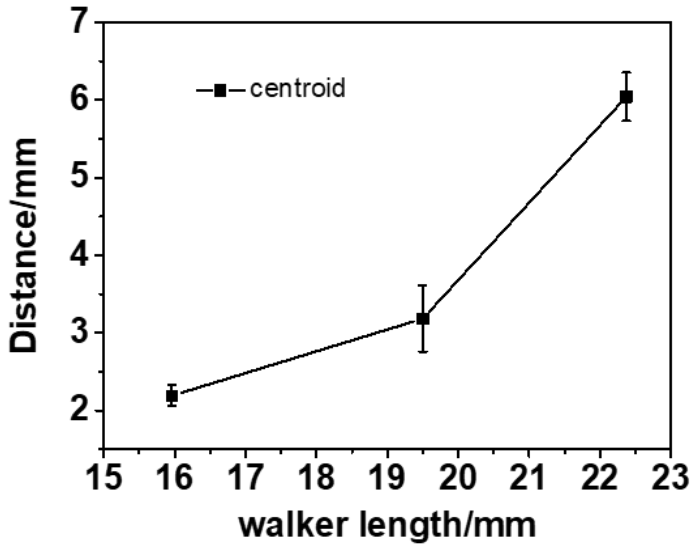

Supplementary Figure 42 Distance of centroid movement for PA hybrid crawlers made of nitro-spiropyran with different body sizes. Error bars represent standard deviations of data collected from three separate samples.

Improved actuation speed by scaling down

Since the contraction and expansion of hydrogels is related to water diffusion, which relies directly on the size and shape of the hydrogel, we anticipate that the actuation speed of hydrogel could be accelerated by scaling down the hydrogel samples. Therefore, we prepared a thinner hydrogel film (0.15 mm thick) containing the spiropyran moiety without the nitro substituent and cut it into a smaller four-arm crawler (10 mm in length) using a flower-shaped template. This crawler was put on the same ratcheted surface and irradiated with the same blue light (447 nm, 8.9 mW/cm^2). It was found that the bending-flattening process was complete in 2 min, which was 20 times faster than that of hydrogel samples with a thickness of 0.5 mm (which took 40 min). Also, the recovery process took 40 min, which was more than two times faster than that of hydrogel films with 0.5 mm thickness (which took 90 min).

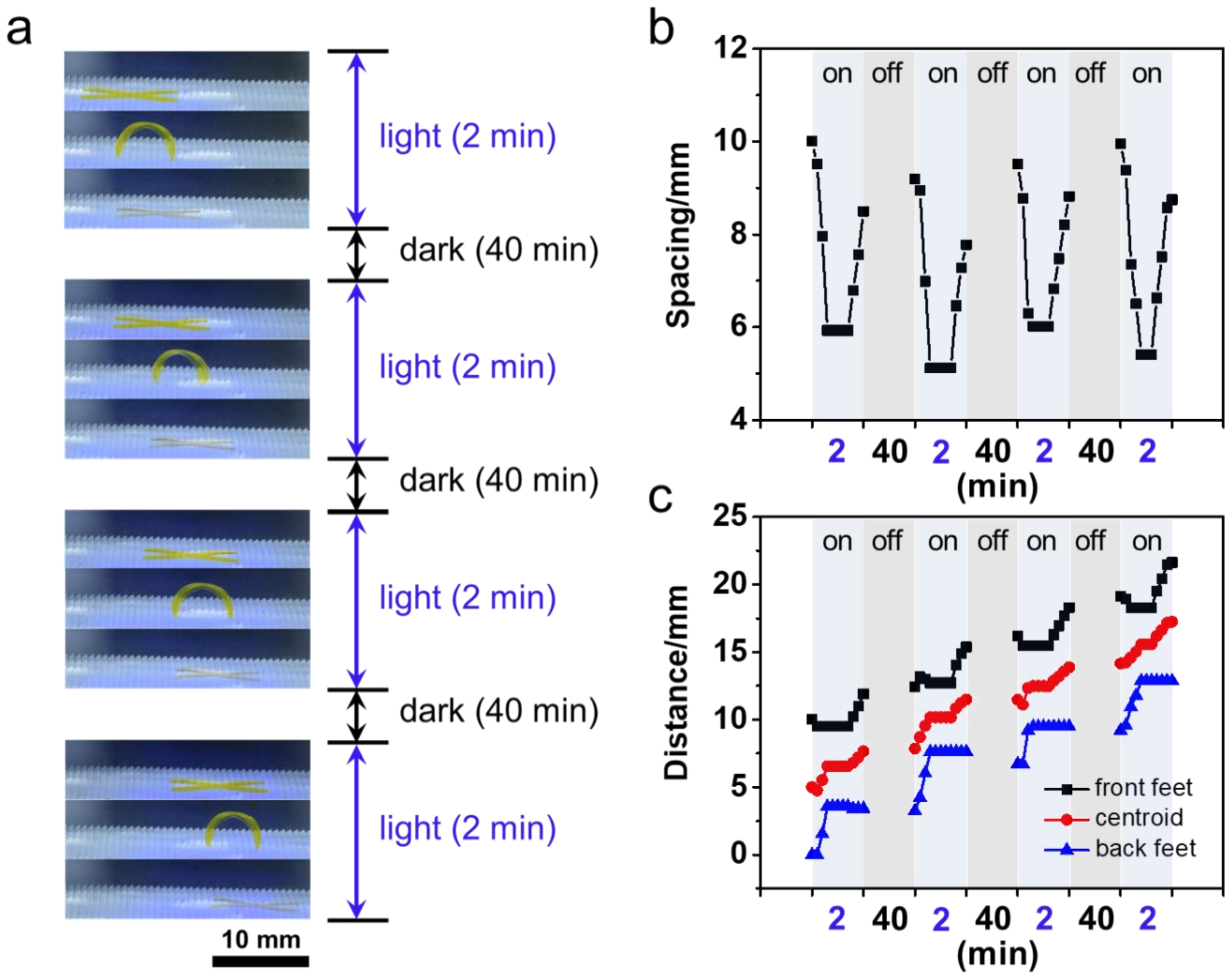

Supplementary Figure 43 Hydrogel crawler with a thickness of 0.15 mm. **(a)** Snapshots of four steps by the object alternating periods of light on and off. The yellow crawler containing spiropyran without the nitro substituent and reswelling in the dark between steps took 40 min. **(b)** Plot of the spacing between the front and back feet during the light (blue, 2 min) period for the crawler made of spiropyran without the nitro substituent. **(c)** Plot of the distance traveled by the front feet (black square), the centroid (red circle), and the back feet (blue triangle) on the ratcheted surface by the hybrid hydrogel during light (blue, 2 min) and dark (gray, 40 min) periods for the crawler made of spiropyran without the nitro substituent.

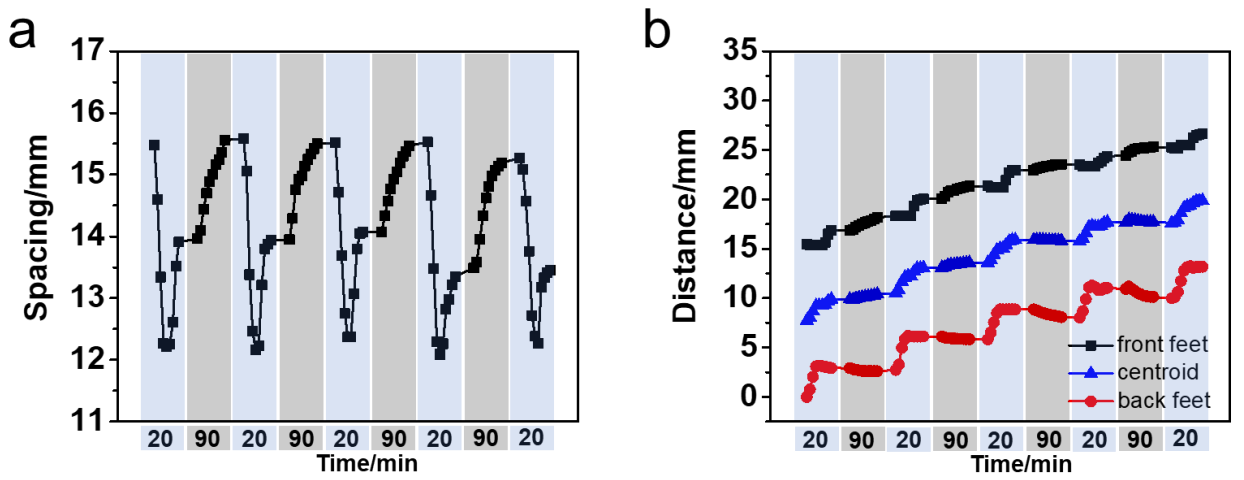

Supplementary Figure 44 (a) Plot of the distance between the front and back feet during light (blue, 20 min) and dark (gray, 1.5 h) periods for the crawler made of spiropyran without the nitro substituent. **(b)** Plot of the distance traveled by the front feet (black square), the centroid (blue triangle), and the back feet (red circle) on the ratcheted surface by the hybrid hydrogel during light (blue, 20 min) and dark (gray, 1.5 h) periods for the crawler made of spiropyran without the nitro substituent.

Cutting parallel, perpendicular and random crawler

A two-layer thin film of PA hybrid hydrogel was printed with 250 μm thickness per layer and a parallel alignment between these two layers. This printed film was cut with a razor blade into either a perpendicular crawler (bending axis perpendicular to filament axis) or a parallel crawler (bending axis parallel to filament axis) according to a cross pattern (white dashed line). The random crawler was cut using the same cross pattern from a cast film.

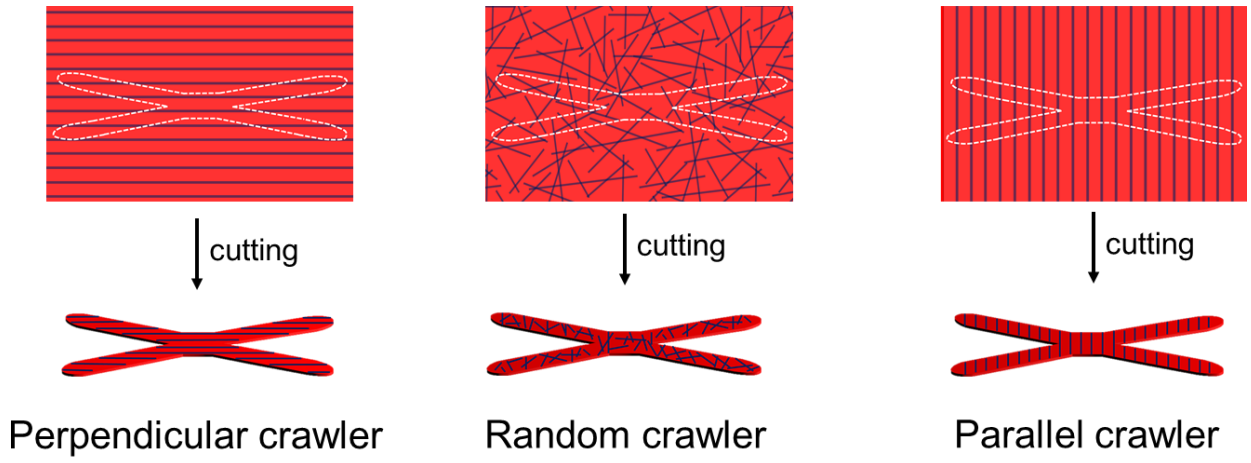

Supplementary Figure 45 Preparation of PA hybrid crawlers with different orientations of the supramolecular PA fibers by 3D printing (left, right) or casting (middle) followed by manual cutting according to a cross pattern (white dashed line).

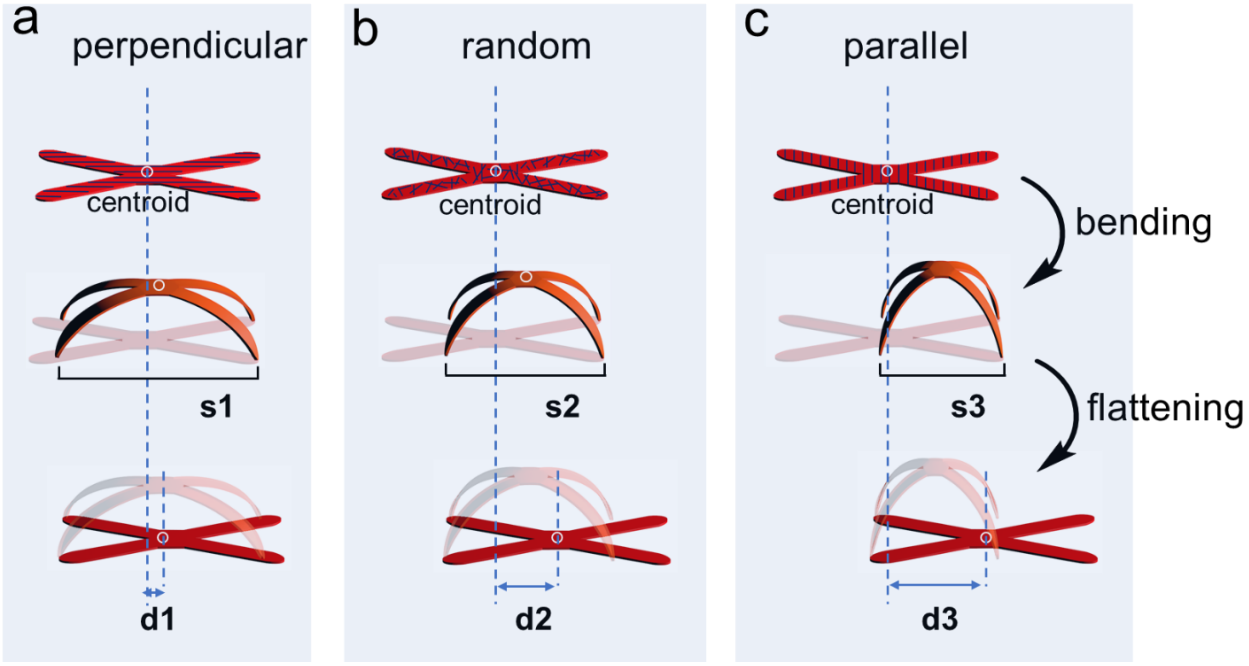

Supplementary Figure 46 Preparation of crawlers with different orientations of supramolecular PA fibers by 3D printing followed by manual cutting. **(a)** The perpendicular crawler with its bending direction perpendicular to filament axis gave the smallest movement of centroid (d1) for one single step. **(b)** The unaligned crawler obtained by casting gave an intermediate movement of centroid (d2) for one single step. **(c)** The parallel crawler with its bending direction parallel to filament axis gave the largest movement of centroid (d3) for one single step due to the anisotropic reinforcement by the aligned PA nanofibers.

Cargo lifting and moving

A rectangular Nylon 66 cargo (black, density 1.14 g/cm^3, 78 mg) was placed on the top of a PA hybrid hydrogel crawler in a flattened geometry and blue light (447 nm, 8.9 mW/cm^2) was applied to the gel from bottom. The cargo could be raised up to 3.5 mm when the crawler popped up in 225 s. A triangle-shaped cargo made of Nylon 66 (12 mg) was attached to the end of a hydrogel ribbon and the light-induced bending of the ribbon lifted the cargo up to 11.5 mm in 340 s. A long strip of the hydrogel was put into a glass channel and an alginate hydrogel bead (10 mg) was put on one side of the stripe. Light was applied locally to the side near the bead and gradually shifted to the other side as the strip curled up, resulting in rolling of the bead over a distance of 42 mm in 265 s.

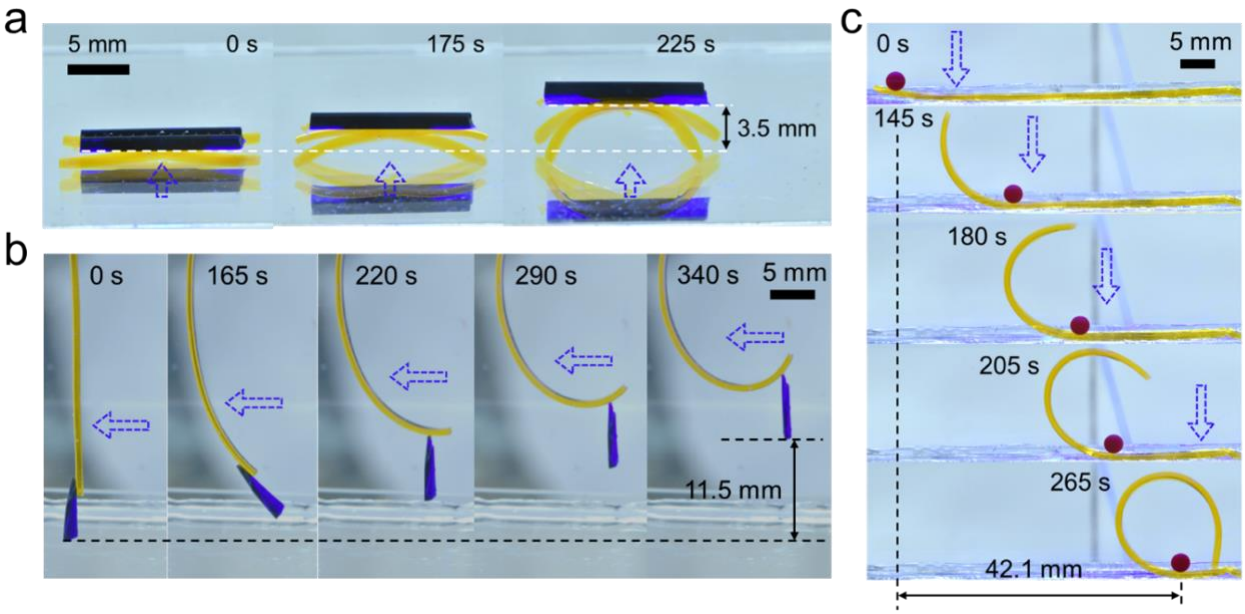

Supplementary Figure 47 Lift and movement of objects by PA hybrid hydrogels. **(a)** The hydrogel crawler raised a rectangular object (78 mg) by popping up once irradiating light from bottom. **(b)** Thin ribbons of the hydrogel bend and lift a cargo (12 mg) that is attached to the end in response to light. **(c)** A strip of the hydrogel moved an alginate bead (10 mg) from left to right over a distance of 42 mm. The alginate bead was colored by a red dye for visualization. Blue dashed arrows indicate the direction of irradiation.

In order to study how hydrophilicity affects the photoactuation behavior of the hydrogel, we synthesized a purely covalent hydrogel in which we replaced 10 mol% of the NIPAM monomers with a more hydrophilic monomer poly(ethylene glycol) methyl ether methacrylate (OEGMA, M_n 500). It was found that this hydrogel displayed a much lower bending angle and slower kinetics relative to the pure PNIPAM hydrogel. No bending was observed with 100% OEGMA, even though the spiropyran moieties retain their photoswitching ability. This suggests that the actuation does not work when the system is too hydrophilic, since the polymer chains are likely extended regardless of the form of the spiropyran moieties.

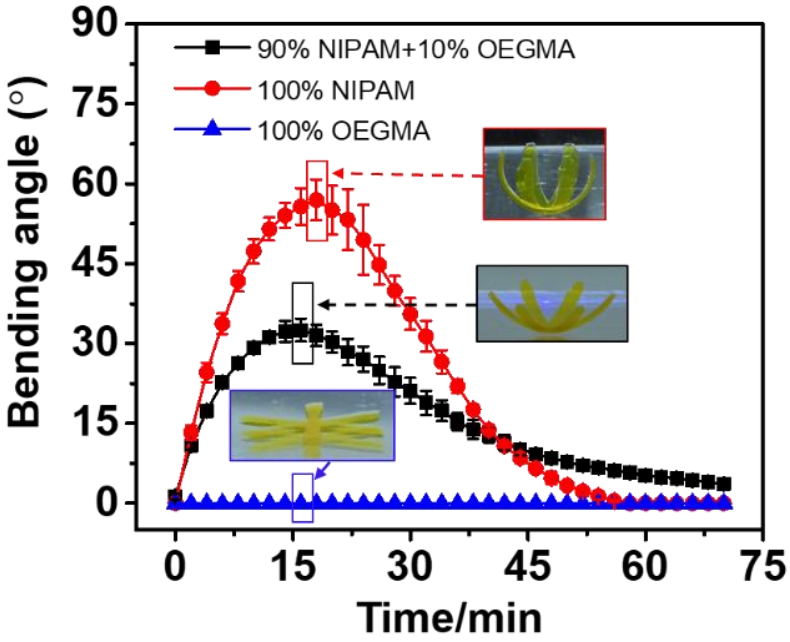

Supplementary Figure 48 Plot of the bending angle vs irradiation time for hydrogel samples made of 10 mol% OEGMA monomer and 90 mol% PNIPAM hydrogel (black), pure PNIPAM hydrogel (red) and pure POEGMA hydrogel (blue). Error bars represent standard deviations of data collected from three separate samples.

Supplementary References

1 Wang, J. M., Wolf, R. M., Caldwell, J. W., Kollman, P. A. & Case, D. A. Development and testing of a general amber force field. *J. Comput. Chem.* **25**, 1157-1174 (2004).

2 Case, D. A.; Betz, R. M.; Cerutti, D. S.; Cheatham, T.E., III; Darden, T. A.; Duke, R. E.; Giese, T. J.; Gohlke, H.; Goetz, A. W.; Homeyer, N.; Izadi, S.; Janowski, P.; Kaus, J.; Kovalenko, A.; Lee, T. S.; LeGrand, S.; Li, P.; Lin, C.; Luchko, T.; Luo, R.; Madej, B.; Mermelstein, D.; Merz, K. M.; Monard, G.; Nguyen, H.; Nguyen, H. T.; Omelyan, I.; Onufriev, A.; Roe, D. R.; Roitberg, A.; Sagui, C.; Simmerling, C. L.; Botello-Smith, W. M.; Swails, J.; Walker, R. C.; Wang, J.; Wolf, R. M.; Wu, X.; Xiao, L.; Kollman, P. A. AMBER 2016, University of California: San Francisco (2016).

3 Lee, O. S., Stupp, S. I. & Schatz, G. C. Atomistic Molecular Dynamics Simulations of Peptide Amphiphile Self-Assembly into Cylindrical Nanofibers. *J. Am. Chem. Soc.* **133**, 3677-3683 (2011).

4 Humphrey, W., Dalke, A. & Schulten, K. VMD: Visual molecular dynamics. *J. Mo.l Graph. Model* **14**, 33-38 (1996).

5 Jorgensen, W. L., Chandrasekhar, J., Madura, J. D., Impey, R. W. & Klein, M. L. Comparison of Simple Potential Functions for Simulating Liquid Water. *J. Chem. Phys.* **79**, 926-935 (1983).

6 Best, R. B. *et al.* Optimization of the Additive CHARMM All-Atom Protein Force Field Targeting Improved Sampling of the Backbone phi, psi and Side-Chain chi(1) and chi(2) Dihedral Angles. *J. Chem. Theory Comput.* **8**, 3257-3273 (2012).

7 MacKerell, A. D. *et al.* All-atom empirical potential for molecular modeling and dynamics studies of proteins. *J. Phys. Chem. B* **102**, 3586-3616 (1998).

8 MacKerell, A. D., Feig, M. & Brooks, C. L. Improved treatment of the protein backbone in empirical force fields. *J. Am. Chem. Soc.* **126**, 698-699 (2004).

9 Phillips, J. C. *et al.* Scalable molecular dynamics with NAMD. *J. Comput. Chem.* **26**, 1781-1802 (2005).

10 Feller, S. E., Zhang, Y. H., Pastor, R. W. & Brooks, B. R. Constant-Pressure Molecular-Dynamics Simulation - the Langevin Piston Method. *J. Chem. Phys.* **103**, 4613-4621 (1995).

11 Martyna, G. J., Tobias, D. J. & Klein, M. L. Constant-Pressure Molecular-Dynamics Algorithms. *J. Chem. Phys.* **101**, 4177-4189 (1994).

12 Darden, T., York, D. & Pedersen, L. Particle Mesh Ewald - an N.Log(N) Method for Ewald Sums in Large Systems. *J. Chem. Phys.* **98**, 10089-10092 (1993).

13 Andersen, H. C. Rattle-a Velocity Version of the Shake Algorithm for Molecular-Dynamics Calculations. *J. Comput. Phys.* **52**, 24-34 (1983).

14 Abraham, M. J.; Murtola, T.; Schulz, R.; Páll, S.; Smith, J. C.; Hess, B.; Lindahl, E., GROMACS: High performance molecular simulations through multi-level parallelism from laptops to supercomputers. *SoftwareX*, **1-2**, 19-25 (2015).

15 Hess, B., Bekker, H., Berendsen, H. J. C. & Fraaije, J. G. E. M. LINCS: A linear constraint solver for molecular simulations. *J. Comput. Chem.* **18**, 1463-1472 (1997).

16 Yesylevskyy, S. O., Schafer, L. V., Sengupta, D. & Marrink, S. J. Polarizable Water Model for the Coarse-Grained MARTINI Force Field. *Plos Comput. Biol.* **6** (2010).

17 Lee, O. S., Cho, V. & Schatz, G. C. Modeling the Self-Assembly of Peptide Amphiphiles into Fibers Using Coarse-Grained Molecular Dynamics. *Nano Lett.* **12**, 4907-4913 (2012).

18 Marrink, S. J., Risselada, H. J., Yefimov, S., Tieleman, D. P. & de Vries, A. H. The MARTINI force field: Coarse grained model for biomolecular simulations. *J. Phys. Chem. B* **111**, 7812-7824 (2007).

19 Caleman, C. et al. Force Field Benchmark of Organic Liquids: Density, Enthalpy of Vaporization, Heat Capacities, Surface Tension, Isothermal Compressibility, Volumetric Expansion Coefficient, and Dielectric Constant. *J. Chem. Theory Comput.* **8**, 61-74 (2012).

20 Grossfield, A. WHAM: an implementation of the weighted histogram analysis method, 2.0.9.